



**IMPROVING THE OPERATIONAL PERFORMANCE OF WIND TURBINE
ROTORS, BY USING VORTEX-TRIPPING DEVICES AS A PASSIVE CONTROL
METHOD**

by

SAVARION COLE MOODIEN

Dissertation submitted in partial fulfilment of the requirements for the degree

Master of Engineering in Energy

In the Faculty of Engineering and the Built Environment

at the Cape Peninsula University of Technology

Supervisor: Dr. Marco Adonis

Bellville


June 2024

CPUT copyright information

The dissertation/thesis may not be published either in part (in scholarly, scientific, or technical journals), or as a whole (as a monograph), unless permission has been obtained from the University

DECLARATION

I, Savarion Cole Moodien, declare that the contents of this dissertation represent my unaided work and that the dissertation has not previously been submitted for academic examination towards any qualification. Furthermore, it represents my own opinions and not necessarily those of the Cape Peninsula University of Technology.



Signed

15 September 2024

Date

ABSTRACT

Wind energy has become one of the major contributors to renewable and sustainable energy in modern times. Since wind turbines were built to produce electricity commercially, engineers have focused on improving their design and efficiency. An increase in efficiency makes for a shorter return on investment timeline, making it a better investment and allowing electricity to be sold at affordable prices. This research study focused on improving the aerodynamic efficiency of wind turbines, using vortex-tripping devices like boundary layer fences specifically. Using boundary layer fences on wind turbine blades has proven to increase the performance of test turbines by 3 to 9%. This study focuses on finding the most effective placement, quantity, and design dimensions for boundary layer fences (blf) for two commonly used NREL wind turbine rotors. The effective design, placement, and quantity of boundary layer fences aim to increase the wind turbine output performance in each of the wind turbines presented. The results achieved were 11.86% for rotor 1 and 9.33% for rotor 2 using the Single Fence Augmentation (SFA) method, and an added 1% on both rotors if the Dual Fence Augmentation (DFA) method is implemented. The key objective was to derive a standard method of improving modern wind turbine rotor aerodynamic efficiency, as a quick installation method, without requiring extensive research and calculations. These methods can be used on units currently in service, to improve and recover lost efficiency and on newly designed units as improvement methods.

KEYWORDS

Wind turbine, rotor blade, rotors, aerodynamic optimization, aerodynamic improvement, boundary layer fences, wing fences, vortex tripping device, aerofoil, angle of attack, rotor optimization, aerodynamics

ACKNOWLEDGEMENTS

I wish to thank:

- My wife, Dr. Renay Moodien for her absolute and unrivalled support.
- My sons, Broden Khai, Jovi Jude, Elih Jole, and Zachary Cole for allowing me to skip a few family days.
- My supervisor, Dr. Marco Adonis for his guidance on this journey.

DEDICATION

I would like to dedicate this dissertation to my late Grandparents, Clifford, and Vena Moodien. I wish I had taken this journey earlier.

For Mamma & Dedde

“...Dankie vir die swaarkry...”

GLOSSARY

Boundary-Layer Fence	A vortex-tripping device is used to delay flow separation on aircraft wings.
Return of Investment	The time it takes to pay back an investment made.
Methodology	The method used to determine future values to make productive predictions.
Aerofoil	The cross-sectional shape of an aerodynamic device where the lift is a major function like a wind turbine blade or aircraft wings.
Lift	The mechanical aerodynamic force is created by the difference in pressure below and above the aerofoil.
Trailing edge	The rear point of the aerofoil.
Airflow	Moving air.
Leading-edge	The frontal edge of the aerofoil.
Stalling	When the critical angle of attack is reached, no further lift can be created.
Wingtip device	An upward curved tip of an aeroplane wing for the prevention of high-pressure air from flowing over and under the wing. Vortex shedding.
Vortex generators	Aerodynamic devices are used to reduce flow separation and delay stalling.
Coefficient of friction	The dimensionless ratio describes the forces between bodies in opposite emotional directions.
Laminar flow	Smooth and balanced flow velocity with little or no mixing between flow layers.
Turbulent flow	Chaotic changes in pressure and flow velocity.
Separation	In aerodynamics, where the flow moves away from the aerodynamic body.
Chord length	The distance between the leading edge and the trailing edge of the aerofoil.
Blade length	The length of the blade from the root to the tip.
Angle of attack	The angle where the relative wind meets the aerofoil to create lift.

ABBREVIATIONS

blf	Boundary Layer Fence
CFD	Computation Fluid Dynamics
Re	Reynolds number
SFA	Single Fence Augmentation
HAWT	Horizontal Axial Wind Turbine
C_p	Coefficient of Power
VG	Vortex Generator
kW	Kilo Watt
kWh	Kilo Watt-hours
MW	Mega Watts
MWh	Mega Watt-hours
NREL	National Renewable Energy Laboratory
3D	Three dimensional
SAWEA	South African Wind Energy Association
IPP	Independent Power Producer
W	Watts
DFA	Dual Fence Augmentation
m/s	Meter per second
m²	Meter squared – Area
RPM	Revolutions Per Minute
AoA	Angle of Attack
N	Newton – Force

TABLE OF CONTENTS

DECLARATION	ii
ABSTRACT	iii
ACKNOWLEDGEMENTS	iv
DEDICATION	v
GLOSSARY	vi
ABBREVIATIONS	vii
TABLE OF CONTENTS	viii
LIST OF FIGURES	1
LIST OF TABLES	4
LIST OF EQUATIONS	5
1. CHAPTER ONE	6
INTRODUCTION	6
1.1 Introduction and background of wind turbine improvements.	6
1.2 Problem Statement	8
1.3 Aims & Objectives	9
1.4 Significance of the Research	9
1.5 Organisation of the Thesis	10
2. CHAPTER TWO	12
LITERATURE REVIEW	12
2.1 Boundary Layer Fences	12
2.2 Vortex Generators	13
2.3 Geometry	13
2.4 Surface Texture	15
2.5 Winglets	15
2.6 Augmentation Methods	16
3. CHAPTER THREE	18
BOUNDARY LAYER FENCES	18
3.1 Introduction	18
3.2 The Mechanics of Boundary Layer Fences (blf)	20
4. CHAPTER FOUR	24
RESEARCH METHODOLOGY	24
4.1 Methodology	24
5. CHAPTER FIVE	28
SIMULATION - APPLICATION OF BOUNDARY LAYER FENCES	28
5.1 Blade selected for the initial CFD study.	28
5.2 Computational Fluid Dynamics	29
5.3 Blade selected for the verification/follow-up CFD study	47
5.4 Results	53
6. CHAPTER SIX	56
ECONOMIC IMPROVEMENT IN A SOUTH AFRICAN CONTEXT	56
6.1 Status Quo in South Africa, September 2023	56
6.2 The possible application of the improvement method	58
7. CHAPTER SEVEN	62
CONCLUSION AND RECOMMENDATIONS	62

BIBLIOGRAPHY	65
APPENDICES	70
APPENDIX A: ACTIVE WIND FARMS IN SOUTH AFRICA, 2023	71
APPENDIX B: NREL 400kW BLADE DESIGN.....	72
APPENDIX C: NREL 1000kW BLADE DESIGN.....	73

LIST OF FIGURES

Figure 1-1 : Wind turbine blade sections (Schubel & Crossley, 2012)	9
Figure 3-1: Wing fence concept design - Patent DE700625C (Liebe, 1938).....	18
Figure 3-2 : Liebe’s Fence design (1938) (Wauters et al., 2021).....	19
Figure 3-3 : MiG -15 Fence design (1947) (Wauters et al., 2021)	19
Figure 3-4 : Furlong & McHugh Fence design (1952) (Wauters et al., 2021).....	19
Figure 3-5 : Haines & Fozard – Harrier Fence design (1967) (Wauters et al., 2021)	19
Figure 3-6 : Wing fence application on aircraft (Flickr, 2023).....	20
Figure 3-7 : Steps of 1D airflow through a wind turbine rotor (Letcher, 2017).....	20
Figure 3-8 : Spanwise airflow diverted/deflected axially by wing fences (Leishman & Gordon, 2023)	22
Figure 3-9 : Vorticity vectors on the surface of a wind turbine blade (Herraez et al., 2016) ..	23
Figure 3-10 : Aerofoil at various angles (Electrical Academia, 2018).....	23
Figure 5-1 : NREL 400kW blade – Attached to a generic hub (Cheney & Migliore, 1999)	28
Figure 5-2 : NREL 400kW blade – Showing aerofoil makeup and a twist of the blade (Author’s work).....	29
Figure 5-3 : Practical Torque explanation (Chegg, 2023)	30
Figure 5-4 : NREL 400kW blade – Mesh for CFD (Author’s work).....	30
Figure 5-5 : NREL 400kW blade – Showing CFD airflow applied perpendicular to the blade (Author’s work).....	32

Figure 5-6 : 400kW NREL - Baseline performance at all selected wind speeds (Author's work).....	32
Figure 5-7 : NREL 400kW blade – Showing the location of the fence installation = 50% of the full length from root to tip (Author's work).....	33
Figure 5-8 : NREL 400kW blade – Showing aerofoil section at 50% of blade length with 5% augmented fence (Author's work).	34
Figure 5-9 : NREL 400kW blade – Showing aerofoil section at 50% of blade length with 10% augmented fence (Author's work).	35
Figure 5-10 : NREL 400kW blade – Showing aerofoil section at 50% of blade length with 15% augmented fence (Author's work).	36
Figure 5-11 : NREL 400kW blade – Showing aerofoil section at 50% of blade length with 20% augmented fence (Author's work).	37
Figure 5-12 : NREL 400kW blade – Showing aerofoil section at 50% of blade length with 25% augmented fence (Author's work).	38
Figure 5-13 : Summary of all blf applied results at AoA =15, showing 20% blf as the best outcome (Author's work).	39
Figure 5-14 : Hand sketch of the selected 20% blf and how it is measured and applied (Author's work).....	39
Figure 5-15 : NREL 400kW blade – Showing the full blade with a 20% augmented fence installed as per the results of the fence height analysis (Author's work).	40
Figure 5-16 : Results of 4m/s performance increase (baseline vs 20%blf @ 0,5L). (Author's work).....	41
Figure 5-17 : Results of 7m/s performance increase (baseline vs 20%blf @ 0,5L). (Author's work).....	41

Figure 5-18 : Results of 10m/s performance increase (baseline vs 20%blf @ 0,5L) (Author's work).....	42
Figure 5-19 : Results of 13m/s performance increase (baseline vs 20%blf @ 0,5L). (Author's work).....	43
Figure 5-20 : Summary of results (baseline vs 20%blf @ 0,5L). (Author's work)	43
Figure 5-21 : NREL 400kW blade – Attached to a generic hub with fences at 50% and 90% of the full length of the blade. (Author's work)	44
Figure 5-22 : NREL 400kW blade – Showing the location of the fence installations = 50% and 90% of the full length from root to tip. (Author's work).....	45
Figure 5-23 : NREL 400kW blade – Showing the full blade with 20% augmented fences installed as per the results of the fence height analysis. (Author's work).....	45
Figure 5-24 : NREL 400kW blade – Showing aerofoil section at 90% of blade length with 20% augmented fence. (Author's work)	46
Figure 5-25 : NREL 1000kW blade – Attached to a generic hub (Velazquez et al., 2014)	47
Figure 5-26 : NREL 1000kW blade – Showing CFD airflow applied perpendicular to the blade. (Author's work).....	48
Figure 5-27 : NREL 1000kW blade – Attached to a generic hub. (Author's work).....	49
Figure 5-28 : NREL 1000kW blade – Showing aerofoil makeup and a twist of the blade. (Author's work).....	49
Figure 5-29 : 1000kW NREL - Baseline performance at all selected wind speeds. (Author's work).....	50
Figure 5-30 : NREL 1000kW blade – Showing the location of the fence installation = 50% of the full length from root to tip. (Author's work).....	51

Figure 5-31 : NREL 1000kW blade – Showing aerofoil section at 50% of blade length with 20% augmented blf. (Author’s work)	51
Figure 5-32 : NREL 1000kW blade – Improvement results after installing a 20% blf. (Author’s work).....	52
Figure 5-33 : NREL 1000kW blade – Graph showing how the improvement results after installing a 20% blf (Author’s work).	53
Figure 6-1 : Total wind energy capacity in South Africa from 2013 to 2022, (Statista, 2023)	58

LIST OF TABLES

Table 5-1 : 400kW NREL - Tabulated baseline performance at all selected wind speeds (Author’s work).....	31
Table 5-2 : Performance of the baseline vs 5% blf applied at all selected wind speeds at AoA = 15 (Author’s work).....	34
Table 5-3 : Performance of the baseline vs 10% blf applied at all selected wind speeds at AoA = 15 (Author’s work).	35
Table 5-4 : Performance of the baseline vs 15% blf applied at all selected wind speeds at AoA = 15 (Author’s work).	36
Table 5-5 : Performance of the baseline vs 20% blf applied at all selected wind speeds at AoA = 15 (Author’s work).	37
Table 5-6 : Performance of the baseline vs 25% blf applied at all selected wind speeds at AoA = 15 (Author’s work).	38
Table 5-7 : Results of CFDs without a blf installed and the 20% blf installed at turbine blade length $L \times 0,5$, applied to all AoA at wind speed 4m/s (Author’s work).....	40

Table 5-8 : Results of CFDs without a blf installed and the 20% blf installed at turbine blade length $L \times 0,5$, applied to all AoA at wind speed 7m/s. (Author’s work).....	41
Table 5-9 : Results of CFDs without a blf installed and the 20% blf installed at turbine blade length $L \times 0,5$, applied to all AoA at wind speed 10m/s. (Author’s work).....	42
Table 5-10 : Results of CFDs without a blf installed and the 20% blf installed at turbine blade length $L \times 0,5$, applied to all AoA at wind speed 13m/s. (Author’s work).....	42
Table 5-11 : Single Fence Comparison - Results of the CFDs with the installation parameters No blf and Single blf). (Author’s work).....	43
Table 5-12 : Fence Comparison - Results of the CFDs with all the installation parameters in this study (No blf, Single blf and Dual blf). (Author’s work).....	46
Table 5-13 : 1000kW NREL - Tabulated baseline performance at all selected wind speeds. (Author’s work).....	50
Table 5-14 : NREL 1000kW blade – Result comparison between “No blf” and “20% blf” at AoA = 16 Degrees (Critical angle). (Author’s work).....	52

LIST OF EQUATIONS

Equation 3-1 : Mathematical expression of airflow through a wind turbine rotor (Letcher, 2017)	21
Equation 5-1 : Mathematical expression of Single Fence Augmentation method (Author’s work).....	54
Equation 5-2 : Mathematical expression of Dual Fence Augmentation method. (Author’s work).....	54

1. CHAPTER ONE

INTRODUCTION

1.1 Introduction and background of wind turbine improvements.

Wind turbines have evolved over the years, from simple machines that harness wind power to pump water to sophisticated structures that produce electricity. The evolution of wind turbines has been driven by the need for more sustainable, efficient, and cost-effective sources of energy.

The first known windmills were used in Persia around 500 AD. These vertical-axis windmills featured wooden blades that were connected to a vertical shaft. They were primarily used to grind grains and pump water.

In the 12th century, wind power plants began to appear in Europe. These early windmills were used to grind grain, saw wood, and pump water. The design was similar to the Persian vertical axis windmill, with wooden blades attached to a vertical shaft.

The first modern wind turbine was built by Charles F. Brush, an American inventor in 1888. It had a rotor with a diameter of 17 meters and was designed to generate electricity. The rotor of the wind turbine consisted of 144 wooden blades arranged circularly.

In the 1920s, a Danish engineer named Poul la Cour developed the modern windmill. This was an improvement on the traditional windmill design that was commonly used in Europe at the time. It had three blades that were arranged in a horizontal position and were used to generate electricity.

In the late 1940s, the wind turbine industry began to take off due to a combination of factors, such as the need for alternative energy sources post-World War II and government support for research and development. This period saw the development of the first megawatt-scale wind turbine in the United States - the Smith-Putnam wind turbine.

During the 1970s, with the oil crisis making energy prices soar, there was renewed interest in wind energy. Researchers and engineers began to work on improving wind turbine design and performance in response to this renewed interest. The first commercial wind turbines were sold in Denmark and the United States, with the latter leading the total number of wind turbines around the world.

In the 1980s, development of third-generation wind turbines began. These featured a horizontal axis design and an innovative pitch control system that allowed the turbine blades

to adjust their angle dynamically according to wind speed. This improved the efficiency of the turbines while also reducing stress on the blades.

The introduction of variable speed control systems in the 1990s was a significant step forward in wind turbine technology, improving efficiency and reducing the cost of electricity generated by wind.

Over the last two decades, wind energy has been one of the fastest-growing industries worldwide. Fourth-generation wind turbines have greater efficiency, increased capacity, and better safety features. The turbines are now built with larger blades, higher towers, and intelligent control systems that integrate artificial intelligence (AI) and big data analytics.

Today, offshore wind turbines are playing a vital role in meeting the rising demand for renewable energy. The world's largest wind turbines are being built across Europe, with rotor diameters over 164 meters and blades that can reach up to 107 meters in length.

Wind turbines have come a long way since the development of early windmills to provide dependable power for a variety of purposes. Advancements in science and technology have improved their efficiency, safety, and reliability, making them a major source of renewable energy globally. With continued effort and investment, they will remain a key player in the transition towards a sustainable future.

Wind turbines have been used for centuries to capture wind energy and convert it into mechanical energy. However, the design of wind turbines has evolved significantly over the years to enhance their aerodynamic efficiency, and thus their power-generation capacity. In this study, we will explore the history of aerodynamic changes made to wind turbines and their impact on wind energy production.

The earliest wind turbines were designed as simple devices with straight blades that rotated around a horizontal axis. These early turbine designs were largely ineffective as the wind could only deliver power during periods of high velocity. As a result, several efforts were made throughout the 19th century to improve the design of wind turbines.

One of the most significant changes made to wind turbines was the introduction of aerofoils. This was first developed by scientists in France in the 19th century, who found that curved blades were more efficient at capturing wind energy than straight blades. The idea behind using curved blades was to create a pressure difference between the two sides of the blade,

which would result in a net force that would drive the turbine. This aerofoil design became popular in the late 1800s and was used in most turbine designs throughout the 1900s.

Another innovation in wind turbine blade design was the development of variable-pitch systems. Variable-pitch systems were initially developed in the 1920s and allowed wind turbines to operate more efficiently by adjusting the angle of the blades based on the wind speed. This design allowed turbines to maintain a consistent amount of power output over a wider range of wind speeds resulting in an overall increase in efficiency.

In the late 20th century, there was a major shift towards using composite materials like fiberglass and carbon fiber to make wind turbine blades lighter and stronger. These materials allowed designers to create longer and thinner blades without risking structural instability, which could increase the efficiency of the wind turbine. The use of composite materials also allowed for more aerodynamic designs, which could increase the efficiency of the wind turbine even further.

Today, wind turbine design has made significant breakthroughs in aerodynamic design. Modern blade designs include a combination of advanced aerofoils, variable-pitch systems, and the use of composite materials to make the blades lighter and more aerodynamic. Additionally, wind turbines are now being designed with new materials that can change shape and respond to different wind conditions. This dynamic blade geometry enables turbines to adjust their shape depending on the wind speed and direction, resulting in more efficient power generation.

Over the past two centuries, there have been significant improvements to the aerodynamics of wind turbines. These advancements have significantly increased the efficiency of wind turbines, resulting in greater power generation and more energy independence for countries around the world. Moving forward, the use of new materials, dynamic blade geometry, and other advanced technologies will continue to drive the evolution of wind turbines, making them an essential part of our future energy mix.

1.2 Problem Statement

In an ideal situation, the wind impacting a wind turbine flows over the blades, generating power over the full length of the blade. However, when analyzing the airflow over a wind turbine rotor blade, it can be noted that there is an element of the airflow that flows spanwise instead of over the blade that is generally not part of the power generation. In addition to this, the air also flows at an angle over the first section of the blade (root) when rotating, which

causes the root to generate less power than its calculated potential. This means that only 2/3 (midspan and tip) of the turbine blades as depicted in Fig 1-1 are responsible for the majority of power generation.

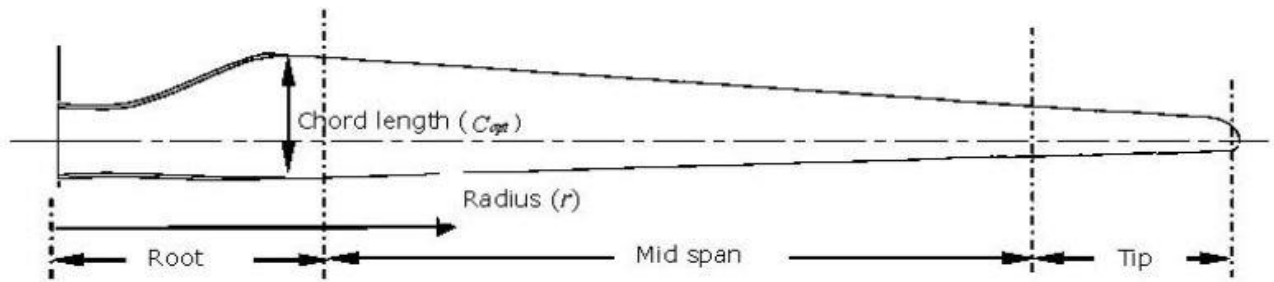


Figure 1-1 : Wind turbine blade sections (Schubel & Crossley, 2012)

1.3 Aims & Objectives

The research aims to develop a standardized method of improving the aerodynamic efficiency of rotor blades of commonly used wind turbine rotors. This study centres around the results obtained from using NREL 400kW and NREL 1000kW rotor blades in a Computational Fluid Dynamic (CFD) study.

The first objective is to determine the most efficient height of the boundary layer fences (blf) at various angles of attack. This objective will be achieved, using CFD analysis of the airflow over the rotors.

The second objective is to position the boundary layer fences (blf) along the length of the wind turbine blade in the most invasive positions. The objective will be achieved when the blf causes enough interruption in the airflow pattern to decrease the drag, delay the stall, and thus increase the thrust of the rotor. From this, a standardized method could then be formulated and mathematically expressed as a final objective.

1.4 Significance of the Research

The focus of this study is to determine if the strategic installation of boundary layer fences, increases the performance of the rotor blades. The specific areas of measuring the performance will be the power output parameters and the start-up wind speed required to rotate the wind turbine. These parameters will be measured at various angles of attack to obtain a panoramic view of the performance improvement.

By improving the performance parameters of a wind turbine, the economic value of the turbine is also improved as well. Wind turbines lose efficiency over the years due to an array

of reasons. By solving this problem, older units can be given their efficiency back and can be economically beneficial in the long run.

1.5 Organisation of the Thesis

The structure of this document intends to take the reader on a progression of the researcher's method of developing, what has been established as the aims and objectives of the research.

Chapter 1

This chapter is an introduction to the all-time physical changes made to wind turbines, as technology discoveries are made. It starts with a brief discussion of the first known windmills built in 500AD and brings the reader to the present day.

This chapter also presents the reader with the problem statement, aims and objectives, and the significance of this research.

Chapter 2

This chapter is aimed at presenting a detailed overview of what has been done in the past to improve the aerodynamic efficiency of wind turbine rotors and the methods and technologies used to gain the results. The focus has been placed on how various vortex-tripping devices or methods have been utilized in research to improve the aerodynamics.

Chapter 3

This chapter provides the reader with a detailed view of what a boundary layer fence is and how they are applied on wind turbine rotors, aircraft, and other systems. This chapter further expands on the background of boundary layer fences, the initial design of the patent and the various designs that followed by various engineers. This chapter also provides the reader with a simplistic explanation of the mechanics of boundary layer fences.

Chapter 4

This chapter outlines the methodology of the research. This chapter describes the various wind speeds, and angle of attack (AoA) used to obtain a baseline for each rotor. This chapter also describes how a single fence is applied to the study, how the ideal boundary layer fence height is established and how it is then applied to the dual fence study.

Chapter 5

This chapter is aimed at providing the reader with detailed insight into how the research was conducted and the results that came from it. This chapter also shares the details of the rotors

used in the study. This chapter also describes the Computational Fluid Dynamics (CFD) method used, the performance baseline of each rotor, determining the ideal fence height and the application of the boundary layer fences. The chapter also presents results obtained from the single and dual fence boundary layer fence application for both rotors.

Chapter 6

This chapter looks at the status quo of the wind turbine industry in South Africa and what the current installation capacity is. It also provides the reader with a simulated estimation of what implementing the researcher's idea could yield in terms of boosting the economic value of the installed wind energy capacity in South Africa in 2023 specifically.

Chapter 7

This chapter concludes the researcher's work, the researcher also presents several recommendations for further work in this field. This chapter also summarizes the results of the CFD study.

2. CHAPTER TWO LITERATURE REVIEW

Over a 40-year wind industry development span, the objectives have always remained constant, a) Improve rotor blade aerodynamic performance b) reduce aerodynamic noise levels and, c) increase structural strength. In the 1980s, fossil fuel producers realized that the reserves were running out, and a push towards wind energy development was launched. This drive has seen exponential advancement in improving rotor blade aerodynamic efficiency, changing the wind energy industry to what it is today (IRENA, 2022). Many advancements of the rotor blades revolved around the design factors of the rotors. However, since there were already hundreds of units in service, some research was done on updating and modifying existing units in situ (Shahan, 2014). Some of the methods developed were copied from modifications made to fighter aircraft during the Second World War to improve handling and increase fuel efficiency. For this literature review the focus is to look at vortex-tripping devices that has a similar function to that of boundary layer fences and how they improve wind turbine rotor aerodynamics.

2.1 Boundary Layer Fences

Wolfgang Liebe, the inventor of the boundary layer fence (blf) or wing fence developed the blf as part of his design work on the Messerschmitt Bf 109B aircraft that was released in 1937 but was modified in 1938 with blf's. Liebe filed a patent in 1938 as a "device for preventing the spread of flow disturbances on aircraft wings" patent DE700625C - Germany. Blfs are described in his pattern as flat plates or flaps. No mention is made of dimensions or methods of deriving dimensions.

Amer et al., (2011) found that the installation of blfs can increase the power output of a horizontal axis wind turbine (HAWT) by 16%. However, this method involved the experimental placing of the blfs and experimental heights were calculated. This experiment was only performed on one rotor blade type. Sreejith (2017) used blfs on an E216 aerofoil experimentally as well. The results were that the drag was reduced by 15.48%, the lift/drag ratio improved by 21.62% @ 6° angle of attack. The trip heights were also investigated experimentally and found after a specific height, the benefits of the blf installation plateaus out.

Sundaravadivel et al., (2013) experimented using an S809 aerofoil blade to determine the best placement of a single blf to increase the power output effectively. It was found that at 50% of the length of the blade, the performance output was the most significant in both

power output (11.8%) and start-up speed. In this study, experimental dimensions were used for the blf height.

2.2 Vortex Generators

Vortex generators (VG) have been used for years on vehicles of all sizes. The performance capabilities in steady flow conditions are relatively well known as opposed to under unsteady conditions. When analyzing VG's, the pressure distributions under both steady and unsteady conditions should be one of the major focuses along with lift, drag, and, momentum in every case of investigation. Each case should have a different flow motion and VG configuration. VG's have proven to be effective in delaying or in some cases, preventing dynamic stalling. For this to be achieved, the correct VG height and configuration or positioning must be perfectly devised.

If VGs are configured correctly, the benefits to aerodynamic performance can be immense. However, if the VGs lose their effectiveness, the rotor blade shows signs of severe losses in the normal coefficient, even larger than that of a clear aerofoil (Tavernier, 2020).

When VGs are positioned closer to the leading edge (LE) of the aerofoil, it has better control space. At 0° , drag increases due to the presence of VG's and due to the earlier transition from laminar to turbulent flow. As flow is applied to the rotor blade with VG's installed, the VG's assist with delaying separation for as long as the VG's can overcome the high adverse pressure gradient at most angles of attack (Tavernier, 2020). Once separation has taken place and the drop in normal coefficient is experienced, the VG's causes the reattachment of flow to be quicker. (Tavernier, 2020).

According to Mueller-Vahl et al., (2012), VG's can ensure a higher rotor torque, which increases the power output. When VGs are installed incorrectly (too close to each other), the undesired drag will increase with the desired lift. Mueller-Vahl et al., (2012) developed a positioning ratio of $x/c = 15-20\%$. Using this ratio, the drag is relatively small to the post-stall lift. VG's can also be used to counteract the effects of mature erosion on rotor blades already in service (Mueller Vahl, 2012). VG height plays a very important role in aerodynamic performance. Mueller-Vahl et al., (2012) found the most effective height to be $H=1.7\%c$.

"c" is the maximum thickness of the aerofoil.

2.3 Geometry

Making a long cavity in a rotor blade works on the same principle as the bumps in a golf ball, it delays flow separation in aerofoil designs and can improve the aerodynamic efficiency

significantly. Experimental studies proved that concaving a section of a rotor blade increased the aerodynamic performance by 3-15%, reducing the sound pressure of the blade's aerodynamic noise by 9.6-15.8%, and increasing the stiffness of the first and second-order vibrations by 7.0 and 4.9% respectively, However, this experiment was done on a small wind turbine blade type, thus whether it is scalable for large wind turbine blade types is unknown at this point. (Jianlong et al., 2019).

Work by Sessarego et al, (2018), compared an NREL 5MW wind turbine blade in its standard straight blade design, to the same blade, swept slightly (2 x different arrangements) at the tip and with a winglet installed on 3rd separate arrangement. These 4 x blade arrangements (Straight, Winglet, Swept-short, and swept-long) were compared at the same inflow conditions. At 8m/s the Swept-short arrangement yielded a decrease in power production of 0.06% and the Swept-long arrangement yielded an increase of 1.4% in power production. At 11.4m/s the Swept-short arrangement yielded an increase in the power production of 0.07% and the Swept-long arrangement yielded an increase of 1.5% in power production.

According to Sugathapala et al., (2020), generally, the design world has a lack of design procedure that specifically targets blades with optimum simplified geometry. They also noted that there is also lack of design of small-scaled wind turbines that cater for wind locations with different parameters.

The shape of the blade and aerofoils used in the design of the blade are imperative for the performance of the blade. Minor changes to the shape have detrimental effects on the blade performance. In modern times the designers do not outline the shape of the blade but rather select aerofoils with known properties to make up a design. NACA or the United States National Advisory Committee for Aeronautics developed aerofoil profiles and catalogued them for design around the time of World War 2. The NACA 44 aerofoil profile was widely used for wind turbines up to 95kW for its robust design properties. Blades developed with the NACA 44 aerofoil had good power and had good stall properties. They were also unaffected by imperfections such as snow or dirt on the blade. The NACA 63 blade was used for wind turbines to the size of 150kW and had a better power curve compared to the NACA 44 profile. However, this profile does not have the same resilience as the NACA 44. The profile is heavily affected by surface imperfections in terms of power production and general performance (The Need Project, 2015)

Work done by Islam et al., (2019) compares NACA and NREL aerofoils and shows that NACA aerofoil profiles have better average performance criteria while the NREL aerofoil has a much better stability criterion.

2.4 Surface Texture

Surface roughness is erosion in high Reynolds Number (Re) aerofoils, but in low Re aerofoils, if distributed over the leading edge (LE) it can have a positive impact when looking at aerodynamic performance. An experiment was conducted on a GA(W)-1 aerofoil, where the effects of distributed hemispherical roughness of different sizes were investigated. The surface pressure and particle image velocimetry were performed under different angles of attack and Re. In all instances, the lift was reduced, and drag increased where LE roughness was applied. When comparing the distribution patterns, the roughness height played a significant role in lift reduction. Large and high roughness patches were found to reduce aerodynamic performance, but lower height roughness patches delayed aerodynamic stall thus, increasing performance at high angles of attack (Yan Zhang, 2017).

Rodrigues et al., (2019) developed a method for increasing the surface roughness of blades, increasing the output power by 8.7% and reducing the aerodynamic noise by 3.5 dB.

Benim et al., (2012) improved the aerodynamic performance of blades by 8%, reducing the sound pressure level of aerodynamic noise by 6.6% by optimizing the structure of the S822 aerofoil. Sanaye et al., (2020) increased the lift-drag ratio of blades by 26%, reducing the blade aerodynamic noise by an average of 1.11% (Jianlong et al., 2019).

2.5 Winglets

Most commonly used on aircraft wings to reduce drag, winglets have been proven to increase the power produced by wind turbines by the RISO National Laboratory in Denmark (Galdamez et al., 2011). This is achieved by lessening the size of the vortex created at the tip of the blade during operation (Johansen & Sorensen, 2006). Results of various literature pieces prove that the implementation of winglets yields positive aerodynamic improvement results on wind turbines. The work by Galdamez et al., (2016) estimated that their design would yield improvement results between 1% and 3%. The results ranged between 0.17% and 7.48% and averaged out at 1.57%.

Work by Sessarego et al., (2018), compared an NREL 5MW wind turbine blade in its standard straight blade design, to the same blade, swept slightly (2 x different arrangements) at the tip and with a winglet installed on 3rd separate arrangement. These 4 x blade arrangements (Straight, Winglet, Swept-short and Swept- Long) were compared at the same inflow conditions. At 8m/s the winglet produced a 1.3% improvement in power production. At 11.4m/s the winglet produced a 0.95% improvement in power production.

Fathi (2020) introduced a spiroid winglet on an NREL 5MW wind turbine to compare it to the standard blade design. The spiroid winglet was designed to have a different twist distribution and camber, pointing towards the suction side of the blade. The idea was to influence the wake vortex near the blade which affects the blade operation. The spiroid winglet had negative results in terms of the vorticity parameters but still yielded an increase in power production.

Different winglet designs in terms of the cant angle and height produce different results. This is clear from the available literature. Work done by Khaled et al., (2019) on a small wind turbine, compared the power production of blades with the cant angle between 15° and 90° . They also compared the winglet height between 1% and 7% of the rotor radius at the optimal angle. The results showed that 6.32% height and 48.3° cant angle were the most optimal winglet. The power co-efficient improvement results were found to be 8.787%. The study was completed using Artificial Neural Network (ANN) as an optimization method.

By solving the incompressible RANS (Reynolds-Averaged Navier Stokes) equation and predicting the inflow air turbulence using the Spalart-Allmaras turbulence model, Hansen & Muhle (2018) found that implementing winglets on conventional wind turbines can yield improvements on the power co-efficient of up to 7.8%. In wind tunnel experiments it can yield results of 8.9% improvement on the power production.

2.6 Augmentation Methods

The process of augmentation is to enlarge or increase the size of an object or system. Over the years, wind turbines have been increasing in size to capture more of the available wind energy in various locations. The method of simply scaling a wind turbine is probably the easiest in terms of plain site innovation. However, it comprises a lot of major design changes and challenges on all fronts of the unit's dimensional and physical parameters. This also comes at a huge cost and is often not feasible. The world's largest wind turbine today (2023) is the Goldwind GWH252-16MW, installed offshore from the Chinese Fujian Province. The unit has a rotor diameter of 252m and has a nameplate capacity of 16MW. This unit broke the record by generating the most power ever generated by a single unit in a single day on 1 September 2023. The unit generated 384.1MWh in only 24 hours after a typhoon hit Southeast China.

While increasing the physical size of the wind turbine has been yielding positive results, engineers are also looking at other innovative ideas for augmentation.

Diffuser Augmented Wind Turbines or DAWT short is one method. By using the Blade Element Momentum or BEM method combined with CFD calculations, the geometry of a rotor in 1-Dimensional analysis, a hypothesis was made to extend Glauert's correction. Using these methods in small wind turbine systems, Chen et al., (2012) augmented a wind turbine with a rotor diameter of only 300mm to produce 164% more power at 10m/s and 111% at 18m/s. In a separate study, using the same methods it was found that the DAWT produced 50% more output power at only 7m/s (Dias do Rio Vaz et al., 2014).

Winds-lenses are diffusers with a flange. It can increase the wind velocity at the rotor plane due to the generation of lower back pressure. Khamlaj & Pumpfkeil (2018) devised a method of optimizing wind-lens efficiency by implementing a multi-objective genetic algorithm or MOGA. This optimization improved the ducted wind turbine and the shape of the diffuser. The results were a reduction in drag and an increase in the power generation capabilities (12.3%). The diffuser efficiency plays a major role in the power output increase and has been verified by researchers using a very similar method (Vaz & Wood, 2018)

The installation of a guide ring is another augmentation method that operates the same as a diffuser but does not guide the airflow inward onto the entire blade area, but rather a section of it. The idea is for the guide ring to divert airflow that would otherwise be lost radially or tangentially, axially onto the blade. For guide rings to be installed on wind turbines, a fine and in-depth analysis of the positioning of the guide ring must be done due to the positioning being very complex. In research conducted by Barnard & Ismail (2022), it was found that at 0.5m/s the 20% position produced negative results, but at 1m/s the 20% position produced a 1% efficiency increase. In the same study, the 15% position produced a 1% increase in efficiency at 0.5m/s and a 24% increase at 1m/s.

3. CHAPTER THREE BOUNDARY LAYER FENCES

3.1 Introduction

Boundary layer fences or blf's are used on aerodynamic devices and wind turbine blades to improve their performance and increase their efficiency. These fences are small protrusions or wires that are placed perpendicular to the flow direction of air, creating a barrier that disturbs the boundary layer and changes the airflow pattern. By reducing the thickness of the boundary layer, boundary layer fences decrease the drag on the surface of the device making it more aerodynamically efficient. In wind turbines, the use of boundary layer fences helps to reduce the turbulence and noise generated by the blades, leading to smoother and quieter operation. The design and placement of boundary layer fences are critical to achieving the desired effect and optimizing the performance of these devices.

The first boundary layer fence, credited to Wolfgang Liebe was the "Liebe Fence", which is described as a protrusion on the upper surface of the aircraft wing (Wauters et al., 2021).

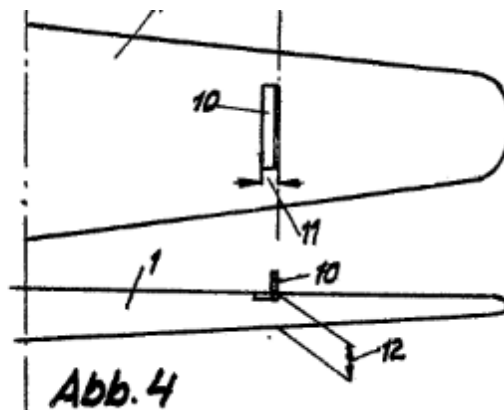


Figure 3-1: Wing fence concept design - Patent DE700625C (Liebe, 1938)

Item "10" is the initial concept used on the Messerschmidt Bf 109B aircraft. Since then many other designs have been derived and used on aircraft.

There are various designs for wing fences as seen in the figures below. However, for this study, a full fence (wrapped around the leading and trailing edges) will be utilized for ease of modeling and CFD meshing.

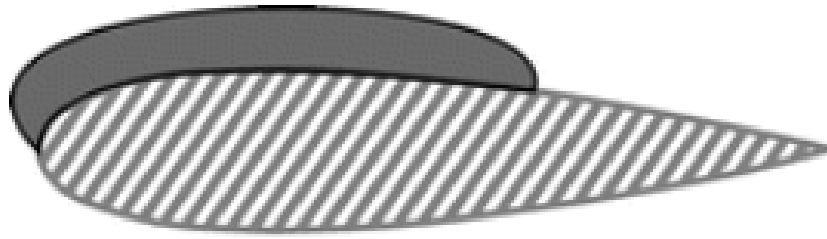


Figure 3-2 : Liebe's Fence design (1938) (Wauters et al., 2021)

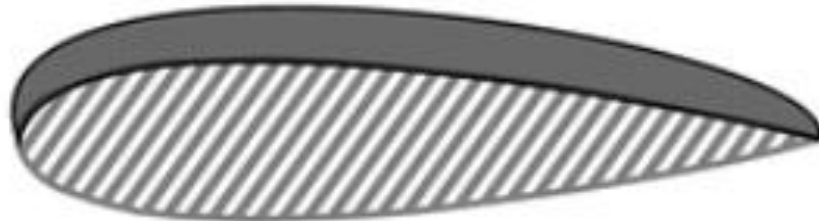


Figure 3-3 : MiG -15 Fence design (1947) (Wauters et al., 2021)

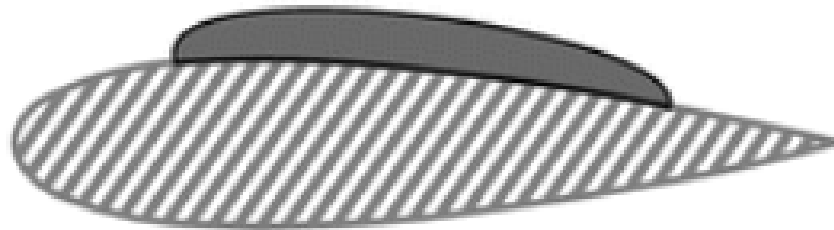


Figure 3-4 : Furlong & McHugh Fence design (1952) (Wauters et al., 2021)

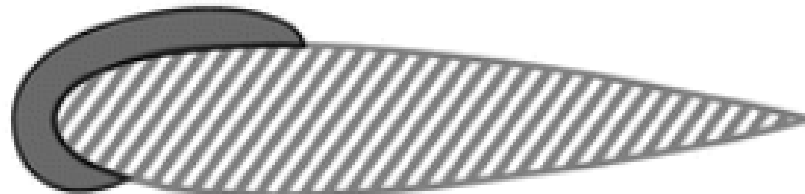


Figure 3-5 : Haines & Fozard – Harrier Fence design (1967) (Wauters et al., 2021)

On aircraft, the wing fences are placed perpendicular to the airflow. The various designs specify the shape, thickness, and height of the fence but are never confirmed by calculation for efficiency. In the pictures below, actual fences can be seen and how they are implemented on aircraft wings. The aerodynamic principle behind wind turbine blades and aircraft wings are the same, hence this application method for fence installation can be applied to wind turbine blades as well.

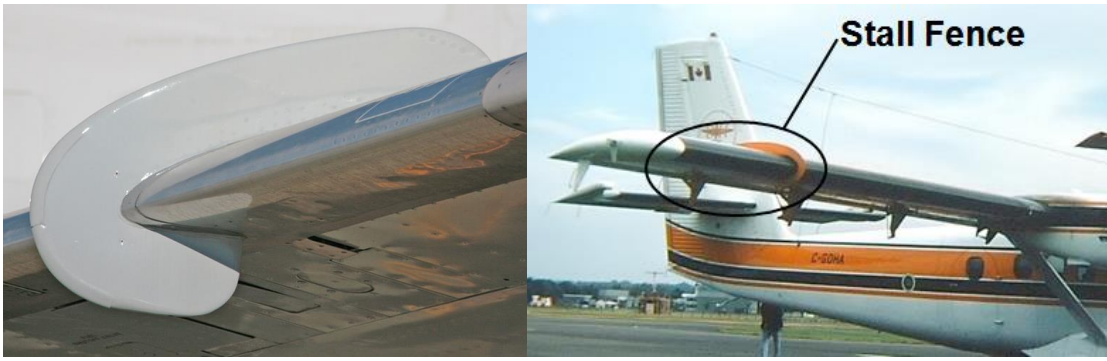


Figure 3-6 : Wing fence application on aircraft (Flickr, 2023)

3.2 The Mechanics of Boundary Layer Fences (blf).

Simplistic Mechanics of how wind turbine rotors work.

The wind turbine rotor captures the power from the wind and converts it to mechanical power. It is made up of a hub and 3 x blades. The kinetic energy is extracted from the air and creates a torque that drives an electrical generator.

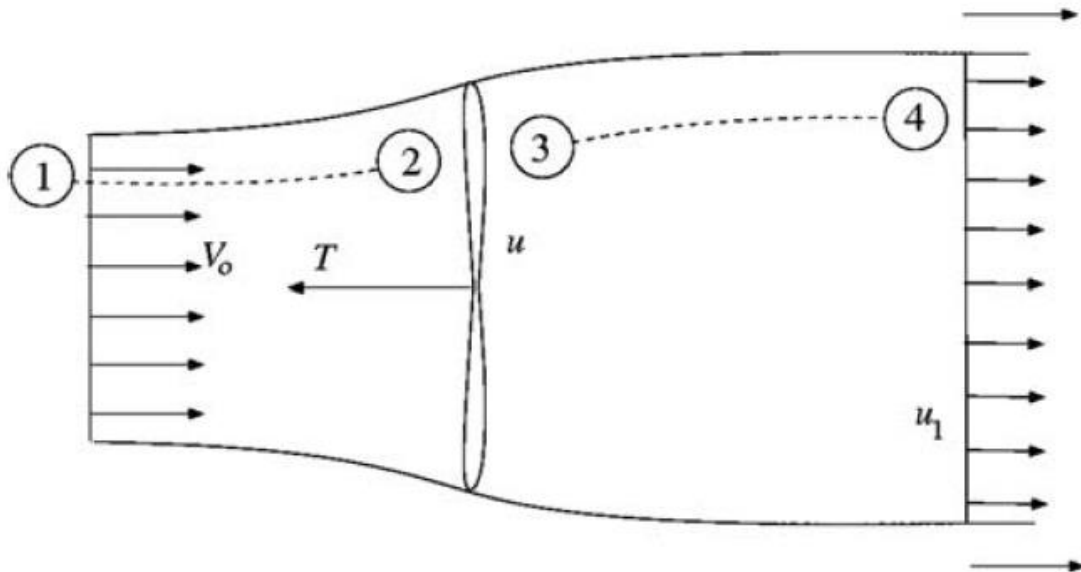


Figure 3-7 : Steps of 1D airflow through a wind turbine rotor (Letcher, 2017)

- i. Step 1, The undisturbed air flows into the rotor
- ii. Step 2, Wind enters the rotor and a thrust force/torque is created
- iii. Step 3, Wind speed is reduced by the extraction of kinetic energy from the wind
- iv. Step 4, Wind exits the rotor and speeds up gradually in the wake.

The formula below describes the process in terms of the physical parameters.

$$P = \frac{1}{2} \dot{m}(V_o^2 - u_1^2) = \frac{1}{2} \rho u A (V_o^2 - u_1^2)$$

Equation 3-1 : Mathematical expression of airflow through a wind turbine rotor (Letcher, 2017)

Where:

P	Power
\dot{m}	Mass flow
ρ	Air Density
V_o	Free wind speed
A	Rotor Area
u_1	Reduced wind speed

How Boundary Layer Fences (blf) works

When the air flows through the rotor, it flows over the wind turbine blades and generates power. The simple formula considers the frontal area of the blades; however, it does not account for the centrifugal forces generated when the rotors are in rotation. Once the rotors rotate, the centrifugal forces create a radial or spanwise component of the airflow, that is not generally considered when calculating the power generation capacity of a rotor (Snel, 1998). According to Butterfield et al., (1990), approximately 30% of the wind turbine blade does not form part of the power generating section. This is normally the section closest to the root of the blade.

In the theory of incompressible flow over finite aircraft wings, the spanwise flow causes vortices to be created near the wing tip. Due to the similar nature of the aerodynamic application on aircraft wings and wind turbine blades, this theory can be applied to analyze the spanwise flow of wind turbine blades as well. The drag on blades normally consists of two elements namely 2D (viscous and pressure) drag and 3D (induced) drag.

The Induced drag is created by the lift force due to the trailing vortex system that follows the blade in rotation. When adding a boundary layer fence to interfere with the spanwise flow on non-rotating systems, the induced drag is reduced, (Sundaravadivel et al., 2013).

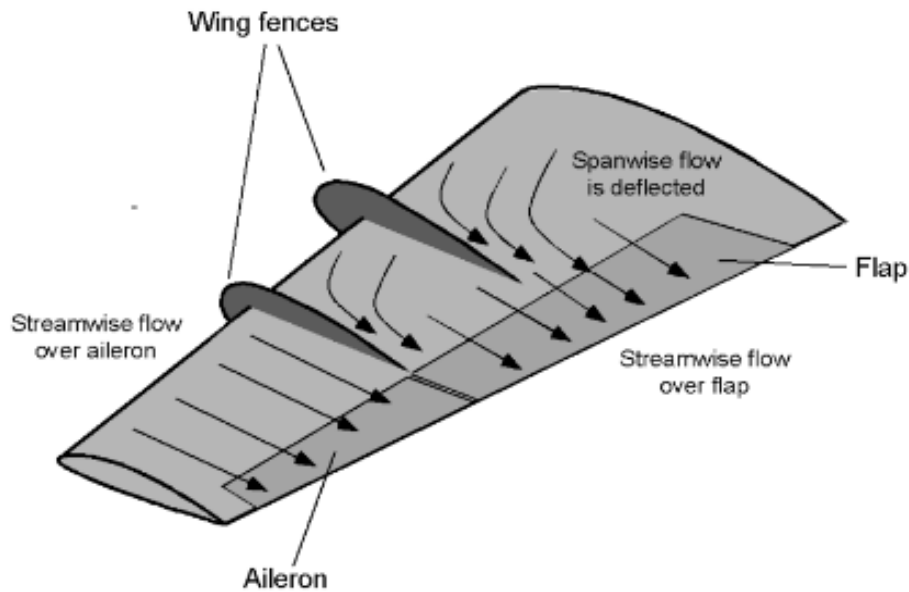


Figure 3-8 : Spanwise airflow diverted/deflected axially by wing fences (Leishman & Gordon, 2023)

The spanwise airflow is very complex at both the root and tip regions of the blade during operation. These regions are greatly affected by the 3D flow that is influenced by the trailing vortices (Micallef, 2012)

The spanwise flow is believed to be the result of 2 x phenomenon:

Spanwise Pressure Gradients – The air is assumed to move from the root to the tip due to spanwise pressure gradients (Schreck et al., 2010)

Centrifugal Force – The force allows for the airflow that is not detached from the blade surface to move outward, toward the tip (Lindenburg, 2003)

As shown below, the centrifugal forces and rotation during operation cause vorticity vectors to form on the surface of the blade. This is a major element in spanwise flow. The wing fence, boundary layer fence, or blf deflects the airflow over the blade, turning it from spanwise or radial flow to axial flow that assists in generating torque or power.

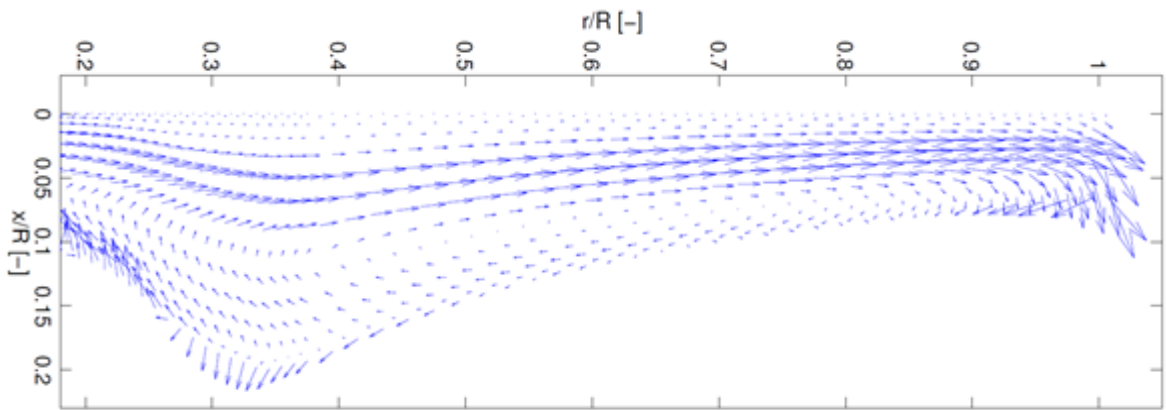


Figure 3-9 : Vorticity vectors on the surface of a wind turbine blade (Herraez et al., 2016)

Stall delay

As the angle of attack (AoA) is increased in rotation with a wind turbine and in flight with an aircraft, so will the lift forces increase. However, at some point during the increase in AoA, the air flowing over the top cambered surface of the aerofoil separates from the surface and forms a wake, the effect of which causes turbulence and results in a significant decrease in lift and an increase in drag forces.

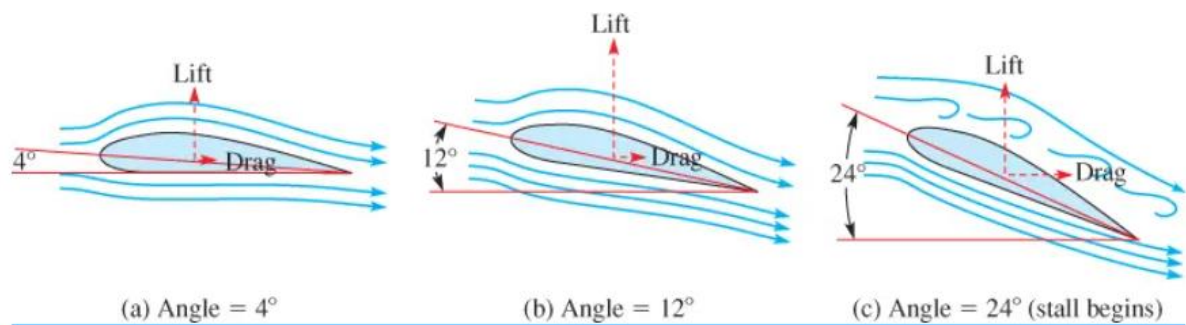


Figure 3-10 : Aerofoil at various angles (Electrical Academia, 2018)

As indicated above, the stall has a specific angle where it will start to occur, depending on the flow medium, wind speed, and Reynolds number. All aerofoils are unique in their design and should have their own AoA at which stall occurs, however, the typical “critical angle” is commonly around 15° (Cooper, 2001).

In aircraft, installing a blf or wing fences on wings significantly increases the “critical angle” which means that the angle at which stall occurs becomes larger, resulting in a more energy-efficient flight (Durga & Balaji, 2016).

4. CHAPTER FOUR RESEARCH METHODOLOGY

The research method utilized was selected due to the reliability and cost-effectiveness of using Computational Fluid Dynamics as a simulation and analysis method. The flow is analyzed in 3D to evaluate the flow over the surface of the blade in the spanwise direction.

4.1 Methodology

- ✓ Select the first blade to be analyzed and modified in the study, the selection will be made based on the available data and the real-world application of the blade.
- ✓ If the blade has all the required dimensional data for the study, then it will be modeled on SolidWorks to create a performance baseline using CFD software.
- ✓ Perform the CFD analysis using the SolidWorks CFD function according to the below method:

$$F = V \times \Phi$$

V = Wind speed entering the rotor

Φ = Angle of attack (AoA)

The cut-in and rated wind speed values will be the first and last wind speeds in the study and will be very important study parameters.

V = 4m/s (V remains constant and AoA must change for every scenario)

- Apply wind from the front at 4m/s and 5°
- Apply wind from the front at 4m/s and 10°
- Apply wind from the front at 4m/s and 15°
- Apply wind from the front at 4m/s and 20°
- Apply wind from the front at 4m/s and 25°

Tabulate the results as $F_a = V_1 \times \Phi_1$; $F_b = V_1 \times \Phi_2$; $F_c = V_1 \times \Phi_3$; $F_d = V_1 \times \Phi_4$

V = 7m/s

- Apply wind from the front at 7m/s and 5°
- Apply wind from the front at 7m/s and 10°
- Apply wind from the front at 7m/s and 15°
- Apply wind from the front at 7m/s and 20°
- Apply wind from the front at 7m/s and 25°

Tabulate the results as $F_e = V_2 \times \Phi_1$; $F_f = V_2 \times \Phi_2$; $F_g = V_2 \times \Phi_3$; $F_h = V_2 \times \Phi_4$

V = 10m/s

- Apply wind from the front at 10m/s and 5°

- Apply wind from the front at 10m/s and 10°
- Apply wind from the front at 10m/s and 15°
- Apply wind from the front at 10m/s and 20°
- Apply wind from the front at 10m/s and 25°

Tabulate the results as $F_i = V_3 \times \Phi_1$; $F_j = V_3 \times \Phi_2$; $F_k = V_3 \times \Phi_3$; $F_l = V_3 \times \Phi_4$

V = 13m/s

- Apply wind from the front at 13m/s and 5°
- Apply wind from the front at 13m/s and 10°
- Apply wind from the front at 13m/s and 15°
- Apply wind from the front at 13m/s and 20°
- Apply wind from the front at 13m/s and 25°

Tabulate the results as $F_m = V_4 \times \Phi_1$; $F_n = V_4 \times \Phi_2$; $F_o = V_4 \times \Phi_3$; $F_p = V_4 \times \Phi_4$

Single Fence

When a baseline has been established, the blade can then be modified by adding a boundary layer fence (blf) to the unit halfway between the root(start) and the tip(end) which will be noted as $L_b \times 50\%$ or $L_{50\%}$ or $0,5L_b$. (Formula $L_b \times \%$ where L_b is the full length of the blade)

The blf has proven to perform best at 50% of the full length of the blade. Hence this modification will only be applied to the proven best result dimension (Arumugam et al., 2016)

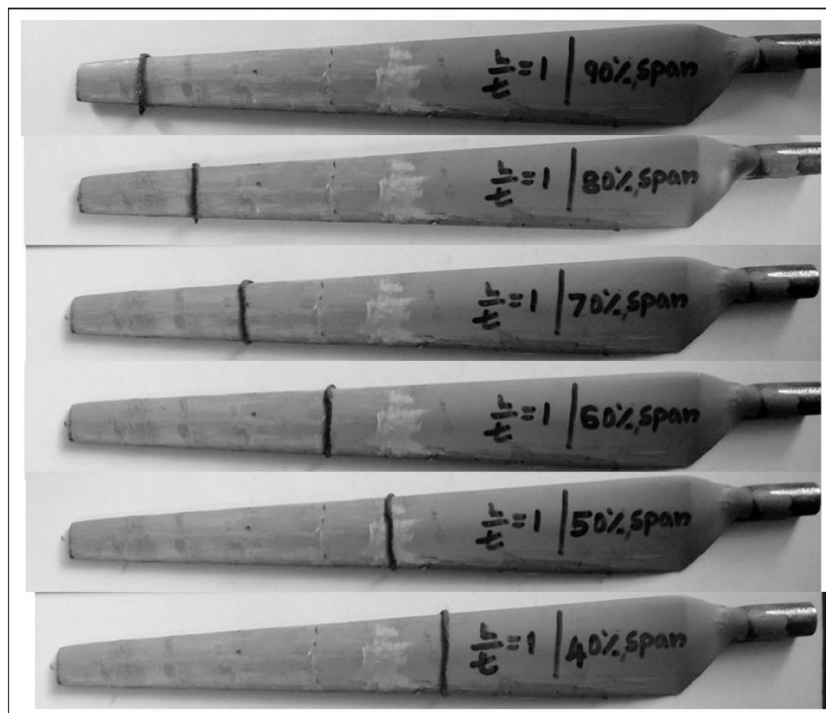


Figure 4-1 : Fences installed at 40% to 90% of blade span for experimental testing (Arumugam et al., 2016)

Fence (blf) Height

The fence height will be determined by increasing the size and finding the most feasible setup in the best-performing scenario. The fence height must be increased in 5% increments from the outer surface of the blade, the thickness or width of the fence has been proven to be of no major significance (Arumugam et al., 2016) (Muheisen et al., 2016).

The increments are determined by using the aerofoil thickness (perpendicular to the camber line) as a reference dimension and installed normally to the aerofoil outline.

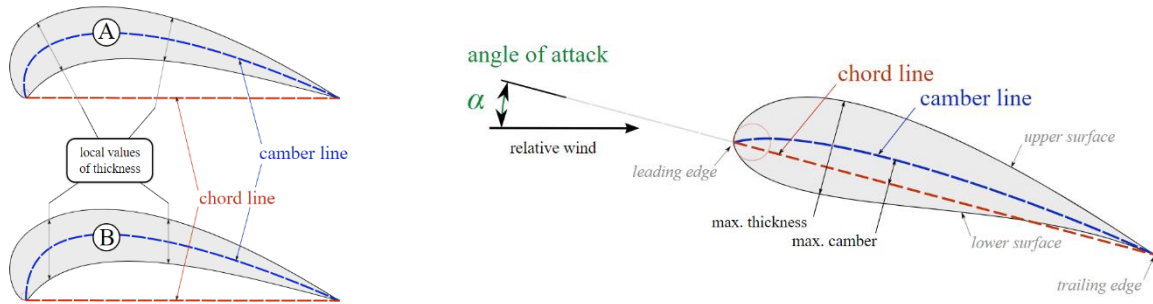


Figure 4-2 : Aerofoil parts (Wikimedia Foundation, 2023)

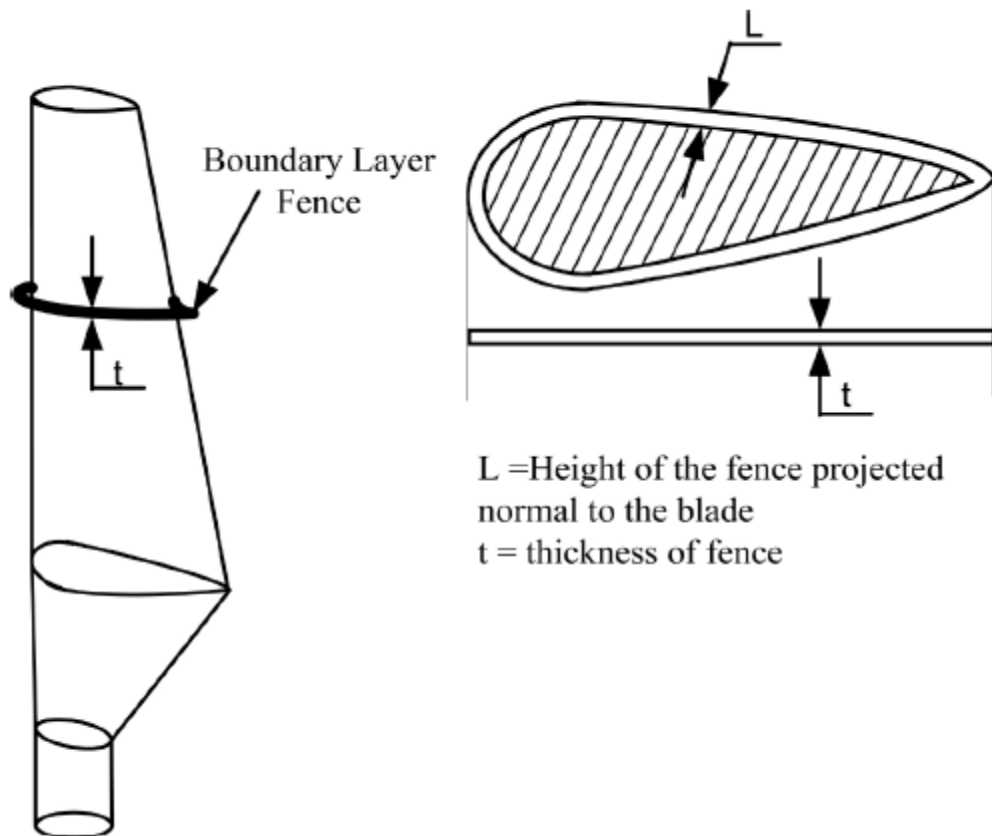


Figure 4-3 : Fence installation illustration (Arumugam et al., 2016)

Once the most feasible fence height has been determined, it will be used in the $0,5L$ position and analyzed in every scenario of $F = V \times \Phi$.

The " $F = V \times \Phi$ " result of the fenced blade can then be compared to that of the unfenced blade.

A mathematical expression, illustrating the single fence augmentation method can then be developed if possible.

Dual Fence

The predetermined fence will be used to analyze whether 2 x fences (disrupting more of the airflow along the blade surface) will yield better performance output than 1 x fence.

According to Durga & Balaji (2016), the application of 2 or more fences does not render significant changes to that of a single fence application. However, we will test this hypothesis.

To position the fences the formula of $L_b \times \%$ will be used.

The fence will be placed at:

- $0,5L_b$ & $0,9L_b$ or at $50\% \times L$ and $90\% \times L$

The fence height will be determined using the same method as in the single fence analysis and applied to the specific blade element where the fence will be placed.

The results of the baseline, single fence, and dual fence augmentations will be compared and tabulated.

If possible, a mathematical expression illustrating the dual augmentation method can then be developed.

Once the results are tabulated and second turbine rotor/blade can be selected, and the same process can be followed to see what the results would be on the second unit.

5. CHAPTER FIVE

SIMULATION - APPLICATION OF BOUNDARY LAYER FENCES

To be able to select an appropriate candidate blade for the research study, all dimensional information should be available for the blade. This information should be able to allow for accurate modeling in SolidWorks or Q-Blade (public source wind turbine blade simulation software).

5.1 Blade selected for the initial CFD study.

Rotor -1 Data

For the research study, the 400kW, National Research Energy Laboratory (NREL) blade with the below detail was selected.

Blade Length	= 15.2m
Aerofoil Profile	= NREL S814 (Root); S812 (Primary Body), S813 (Tip)
Blade Twist	= 45 Degrees between root and tip
Critical Angle	= 15 Degrees
Maximum Chord Length	= 1,9m
Cut-in speed	= 4m/s
Rated speed	= 13m/s
Cut-out speed	= 25m/s
Power Curve	= Not available for the specific unit.
Position of each Blade Element	= Please see "Appendix B"

Information obtained from Cheney & Migliore (1999)

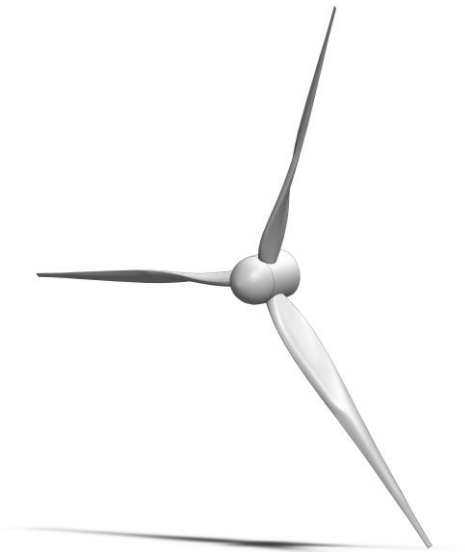


Figure 5-1 : NREL 400kW blade – Attached to a generic hub (Cheney & Migliore, 1999)

The selected NREL 400kW blade has a 45° twist from the root to the tip of the blade. The blade design starts with a cylinder and transitions into a S814 aerofoil for the first 40% of the blade. The second section (40-75%) transitions from an S814 aerofoil to an S812 aerofoil design. The last section (75-100%) transitions from the S812 to a S813 aerofoil.

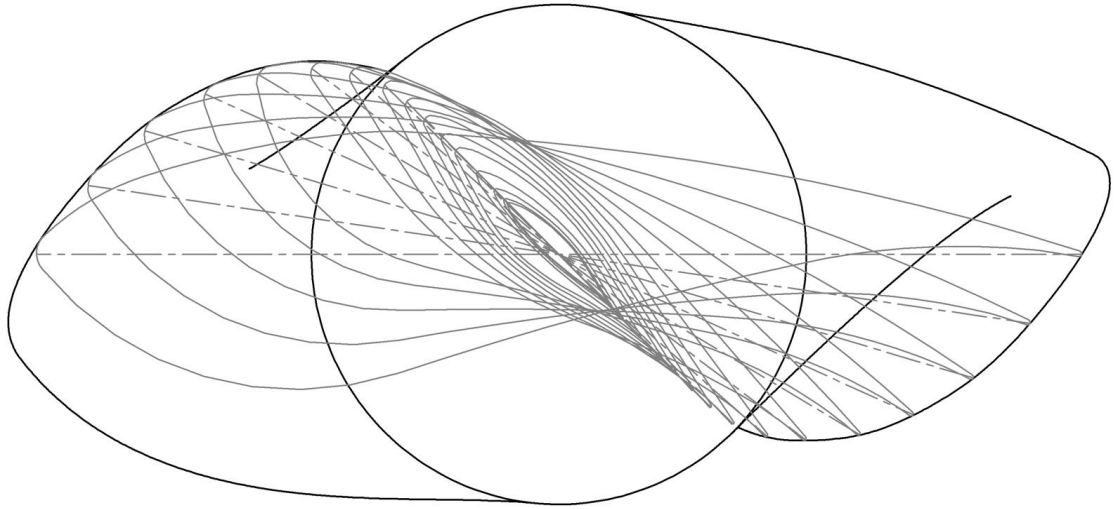


Figure 5-2 : NREL 400kW blade – Showing aerofoil makeup and a twist of the blade (Author’s work)

5.2 Computational Fluid Dynamics

The CFD study is based on simulating fluid flow scenarios to analyze physical phenomena. In this case, the selected blade is put under scrutiny to investigate how it will behave in certain scenarios.

SolidWorks was used for this study as Q-Blade does not allow for modifications to the level that is required for a blf to be installed and analyzed accurately.

The selected CFD test method is a low-speed shaft torque prediction as explained and applied by Simms et al., (2001).

Torque or moment of force is measured when a perpendicular force is applied on a lever around an axis. It can cause an object to rotate and is responsible for angular acceleration. Torque can also be defined as the tendency of a force to twist or turn an object.

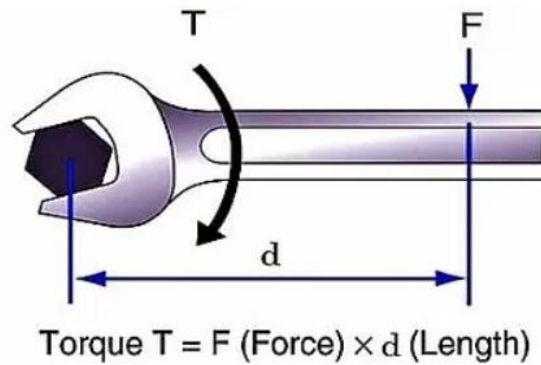


Figure 5-3 : Practical Torque explanation (Chegg, 2023)

For this study, the wind was applied from the front at 90° to the rotor at various speeds (4 -13 m/s), the rotor was kept stationary during the study. As the wind was applied, the angle of attack (AoA) of the blades was changed to various angles (0° - 35°) to create a lift force, which is measured as Torque on the rotor axis. Torque is an element of Power; hence it can be used to predict Power generation.

$$\text{Power (kW)} = \text{Torque (Nm)} \times \text{Angular Speed (rads/min)}$$

CFD Mesh

To be able to accurately analyze the airflow over the blade, a mesh must be selected or generated on SolidWorks. The mesh must be small enough about the blade to be able to render detail from the model. The smaller the meshing, the better and more accurate results will be obtained. However, the smaller the mesh, the longer and more difficult it becomes to compute the results. For this study, a meshing size of 440 x 440 x 440mm structured hexahedral was used.

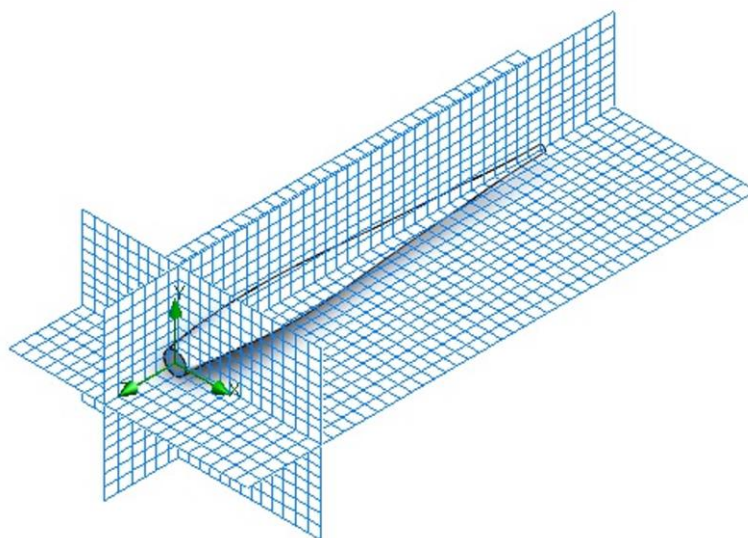


Figure 5-4 : NREL 400kW blade – Mesh for CFD (Author’s work)

Baseline Torque Analysis – Rotor 1

The baseline analysis was conducted to assess the initial output values and characteristics of the turbine blade in its original, unmodified state. According to the datasheet provided, the cut-in wind speed, which is the minimum wind speed required for the turbine to start generating power, is 4 m/s. This wind speed was selected as the first input condition for the baseline performance analysis of the turbine blade. From the results below, even at 4m/s and AoA = 0°, the turbine blade is generating a positive torque on the main shaft. The research method statement or methodology in Chapter 4 only made mention of using AoA = 0°, 5°, 15°, 20°, 25°, 30°, and 35°, however, the decision was made to add 14°, 16°, and 17° to the analysis to show a detailed indication of what happens closer to the stall parameters of the blade.

The baseline analysis was done for each wind speed (4, 7, 10, 13m/s) as indicated in the methodology. Each graph was plotted separately. The airflow was applied perpendicular to the blade.

Table 5-1 : 400kW NREL - Tabulated baseline performance at all selected wind speeds (Author's work)

Baseline Torque Analysis										
V (m/s)	Angle of Attack (AoA)									
	0	5	14	15	16	17	20	25	30	35
4	117,89	243,99	369,01	323,51	309,00	336,33	201,44	178,37	163,26	139,33
7	-86,30	739,88	1117,61	1229,42	653,15	1044,25	619,33	550,21	499,92	425,88
10	734,19	1515,25	2261,93	2031,90	1944,30	2099,93	1261,54	1113,24	1020,50	870,52
13	-317,82	2950,05	3824,55	4214,01	2954,81	2899,70	2121,95	1889,05	1724,98	1467,34

As seen above, even though 4m/s is the cut-in speed, the results show very low torque values at all AoA, but positive nonetheless.

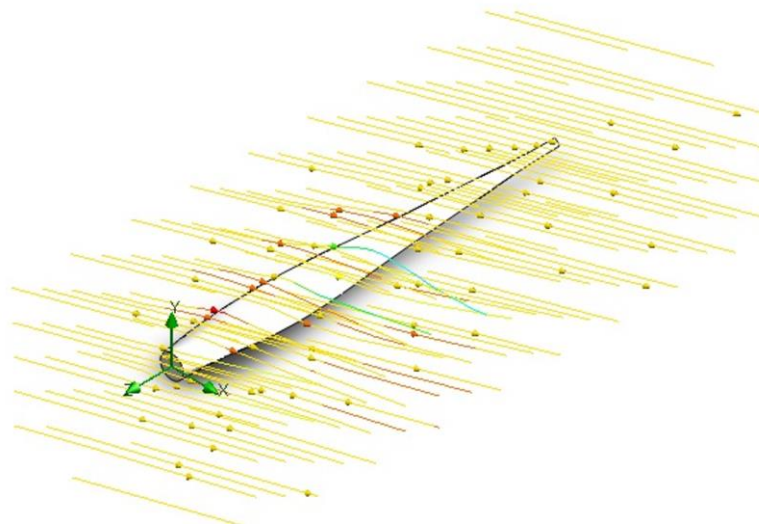


Figure 5-5 : NREL 400kW blade – Showing CFD airflow applied perpendicular to the blade (Author’s work)

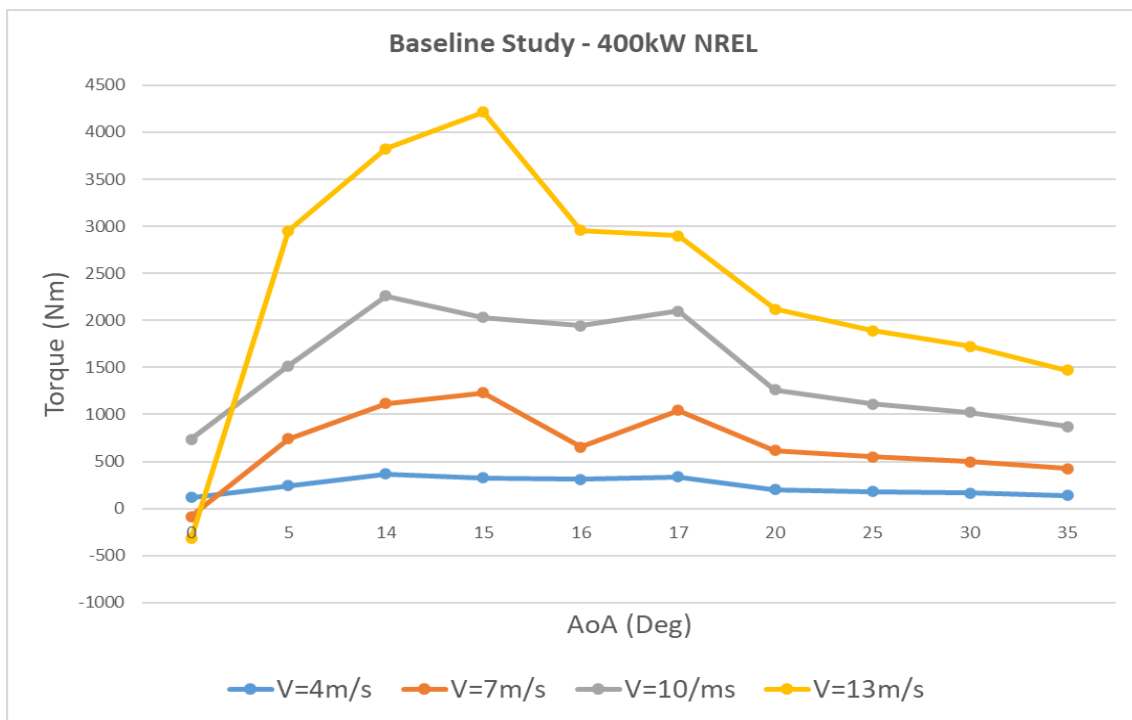


Figure 5-6 : 400kW NREL - Baseline performance at all selected wind speeds (Author’s work)

Fence Height Analysis

The fence height analysis was done based on the output values of the baseline analysis. From the baseline analysis results, it was found that 15° is the critical angle, meaning that the best results were obtained at $AoA = 15^\circ$. Analyzing the fence height at the best-performing output parameters gives the best possible result at maximum torque with the fence installed. The fence height analysis is a comparative study between the baseline with no fence installed and that of an installed fence at various heights (5%, 10%, 15%, 20%, and 25%).

The fence height increments are determined by multiplying the aerofoil thickness with the incremental percentages. For example, if the aerofoil thickness is 100mm then the fence height at 5% will be 5mm ($100\text{mm} \times 5\%$) or 15% will be 15mm ($100\text{mm} \times 15\%$).

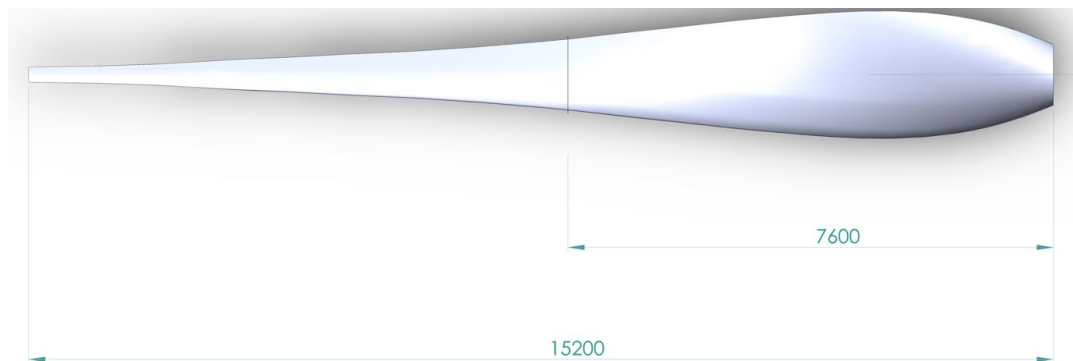


Figure 5-7 : NREL 400kW blade – Showing the location of the fence installation = 50% of the full length from root to tip (Author’s work)

Case 1

In case 1 the aerofoil thickness = 234mm (234 x 5%), 12mm is the height of the fence. The fence is installed around the aerofoil at 50% of the length of the wind turbine blade as stated in the methodology.

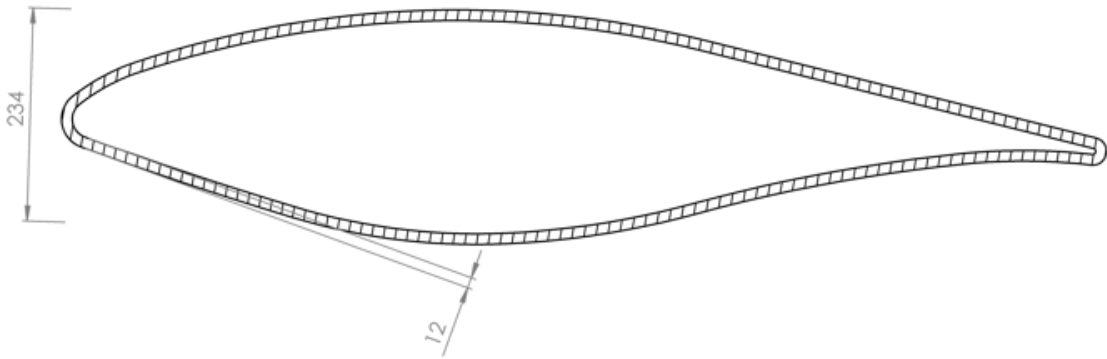


Figure 5-8 : NREL 400kW blade – Showing aerofoil section at 50% of blade length with 5% augmented fence (Author’s work).

At 5% the torque output increased by 4,22% on average.

Table 5-2 : Performance of the baseline vs 5% blf applied at all selected wind speeds at AoA = 15 (Author’s work).

V (m/s)	AoA=15		Increase (%)
	No blf (Nm)	5% blf (Nm)	
4	323,51	341,91	5,38
7	1229,42	1265,87	2,88
10	2031,90	2156,49	5,78
13	4214,01	4337,48	2,85
Average Torque Increase			4,22

Case 2

In case 2 the aerofoil thickness = 234mm (234 x 10%), 23mm is the height of the fence.

The fence is installed around the aerofoil at 50% of the length of the wind turbine blade as stated in the methodology.

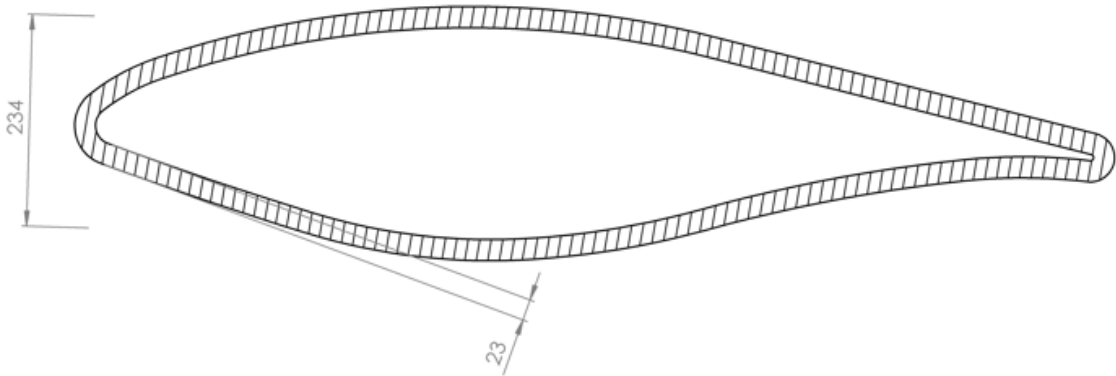


Figure 5-9 : NREL 400kW blade – Showing aerofoil section at 50% of blade length with 10% augmented fence (Author's work).

At 10% the torque output increased by 4,24% on average.

Table 5-3 : Performance of the baseline vs 10% blf applied at all selected wind speeds at AoA = 15 (Author's work).

V (m/s)	AoA=15		Increase (%)
	No blf (Nm)	10% blf (Nm)	
4	323,51	342,99	5,68
7	1229,42	1265,90	2,88
10	2031,90	2151,24	5,55
13	4214,01	4337,52	2,85
Average Torque Increase			4,24

Case 3

In case 3 the aerofoil thickness = 234mm (234 x 15%), 35mm is the height of the fence.

The fence is installed around the aerofoil at 50% of the length of the wind turbine blade as stated in the methodology.

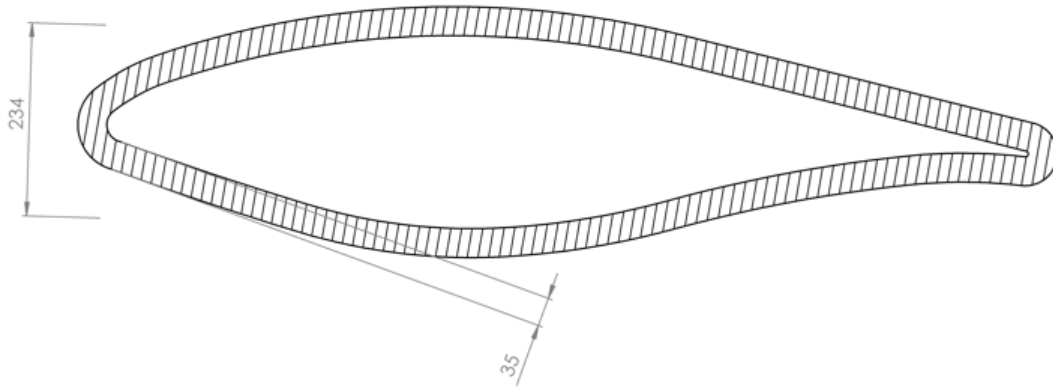


Figure 5-10 : NREL 400kW blade – Showing aerofoil section at 50% of blade length with 15% augmented fence (Author's work).

At 15% the torque output increased by 8,25% on average.

Table 5-4 : Performance of the baseline vs 15% blf applied at all selected wind speeds at AoA = 15 (Author's work).

V (m/s)	AoA=15		Increase (%)
	No blf (Nm)	15% blf (Nm)	
4	323,51	413,33	21,73
7	1229,42	1265,67	2,86
10	2031,90	2151,51	5,56
13	4214,01	4337,85	2,85
Average Torque Increase			8,25

Case 4

In case 4 the aerofoil thickness = 234mm (234 x 20%), 47mm is the height of the fence.

The fence is installed around the aerofoil at 50% of the length of the wind turbine blade as stated in the methodology.

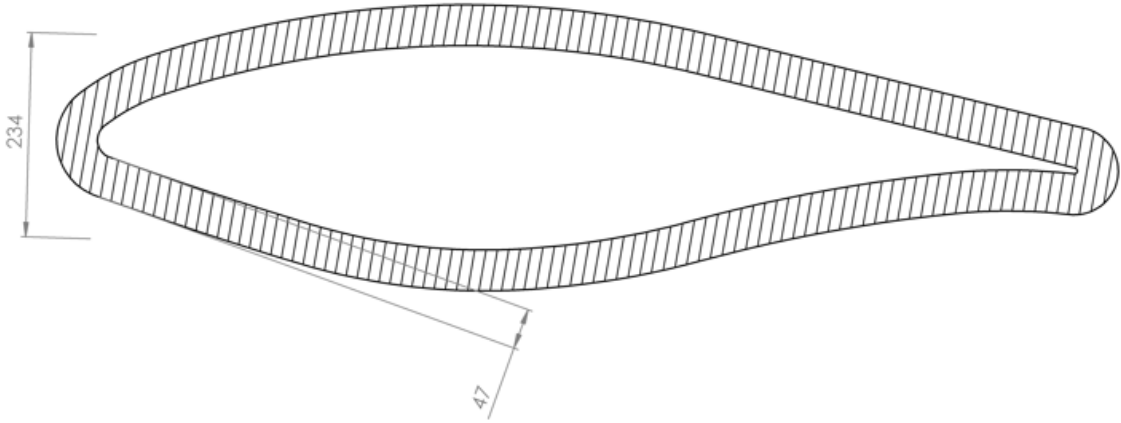


Figure 5-11 : NREL 400kW blade – Showing aerofoil section at 50% of blade length with 20% augmented fence (Author’s work).

At 20% the torque output increased by 11,86% on average.

Table 5-5 : Performance of the baseline vs 20% blf applied at all selected wind speeds at AoA = 15 (Author’s work).

V (m/s)	AoA=15		Increase (%)
	No blf (Nm)	20% blf (Nm)	
4	323,51	411,20	21,33
7	1229,42	1265,31	2,84
10	2031,90	2556,73	20,53
13	4214,01	4333,06	2,75
Average Torque Increase			11,86

Case 5

In case 5 the aerofoil thickness = 234mm (234 x 25%), 58mm is the height of the fence. The fence is installed around the aerofoil at 50% of the length of the wind turbine blade as stated in the methodology.

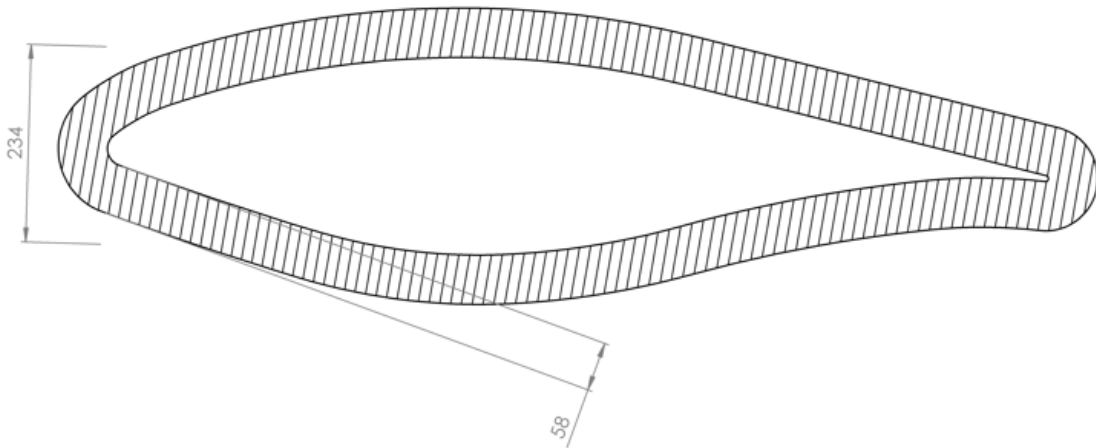


Figure 5-12 : NREL 400kW blade – Showing aerofoil section at 50% of blade length with 25% augmented fence (Author’s work).

At 25% the torque output increased by 11,85% on average.

Table 5-6 : Performance of the baseline vs 25% blf applied at all selected wind speeds at AoA = 15 (Author’s work).

	AoA=15		Increase (%)
V (m/s)	No blf (Nm)	25% blf (Nm)	
4	323,51	410,88	21,26
7	1229,42	1265,32	2,84
10	2031,90	2558,05	20,57
13	4214,01	4332,49	2,73
<i>Average Torque Increase</i>			11,85

Based on the results of the fence height analysis, it can be seen on the below graph that fence 20% presented the best result of 11.86% improvement overall. As the fence height increases, the torque generation improves as well. However, at approximately 20% of the thickness, the improvements evens out. If the height of the fence is above 20% of the aerofoil thickness, the fence is not as optimal as possible.

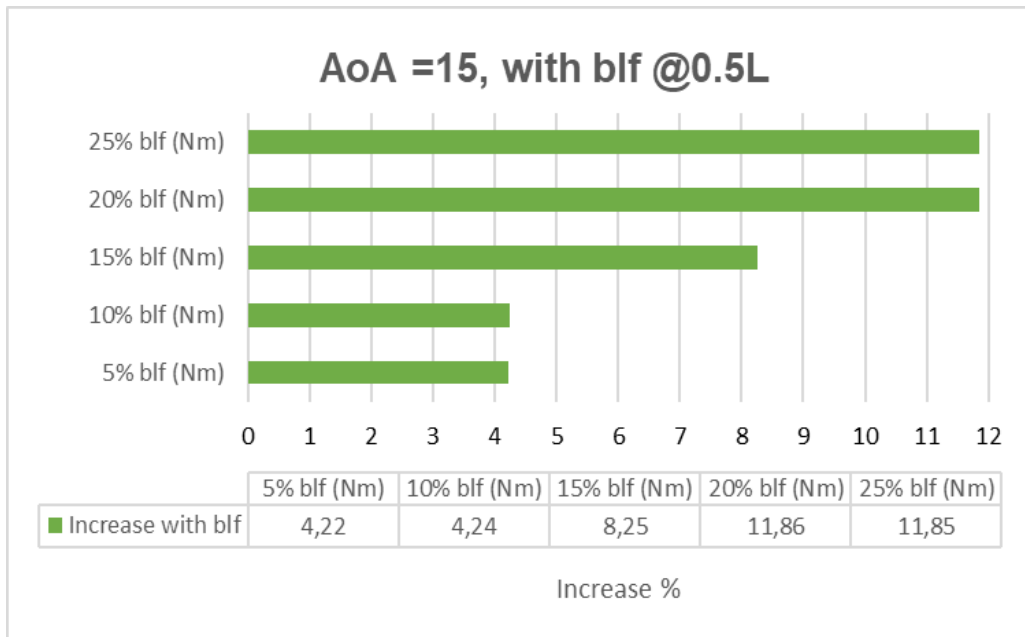


Figure 5-13 : Summary of all blf applied results at AoA =15, showing 20% blf as the best outcome (Author's work).

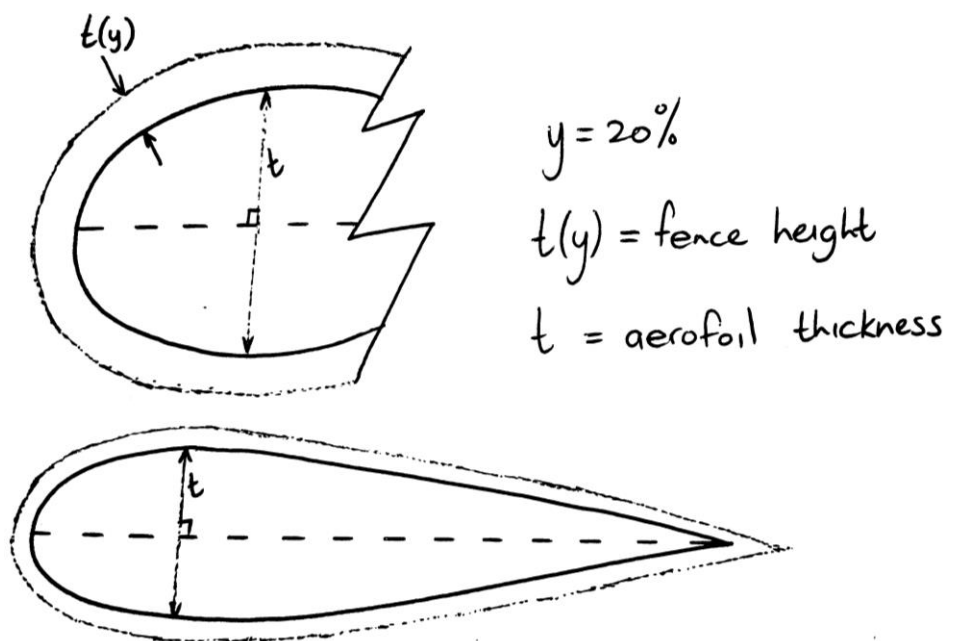


Figure 5-14 : Hand sketch of the selected 20% blf and how it is measured and applied (Author's work).

Single Boundary Layer Fence (blf) Application – Rotor 1

In the below figure, the 3D model shows the fence installed on the blade. The 20% blf looks insignificant but as per results found in the “fence height analysis” section of this study, it is the most optimal height for the objective of capturing the spanwise airflow and converting it to torque.

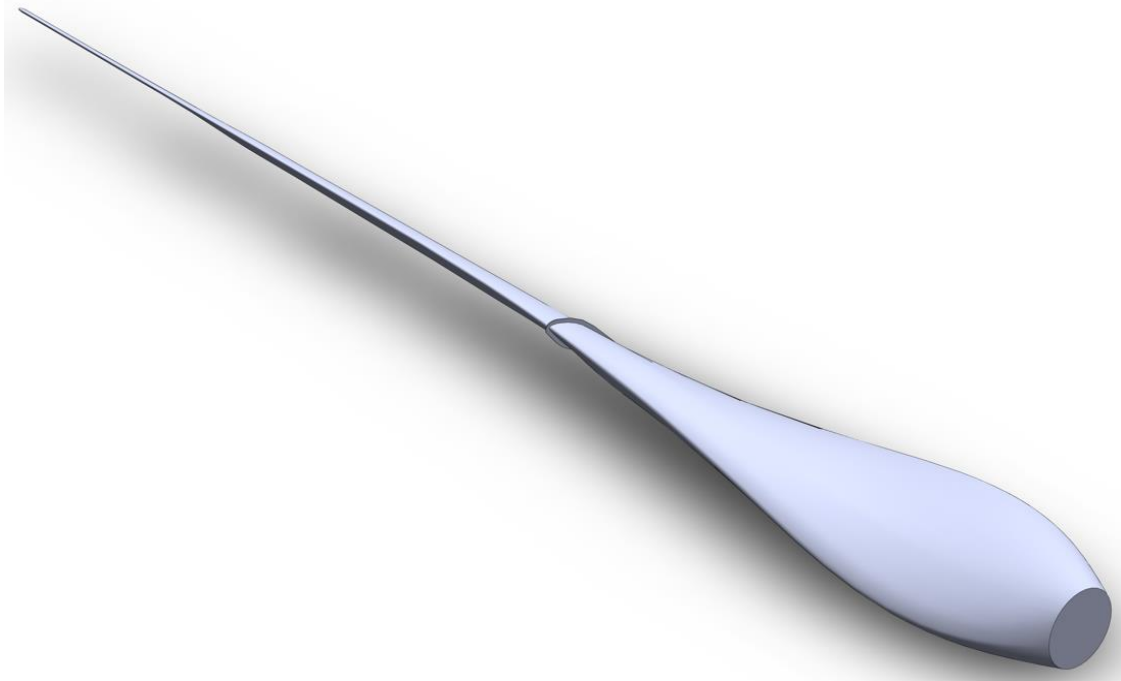


Figure 5-15 : NREL 400kW blade – Showing the full blade with a 20% augmented fence installed as per the results of the fence height analysis (Author’s work).

Table 5-7 : Results of CFDs without a blf installed and the 20% blf installed at turbine blade length $L \times 0,5$, applied to all AoA at wind speed 4m/s (Author’s work).

	20% blf @0.5L, applied to all AoA @ V = 4m/s												V
AoA (Deg)	0	1	5	10	14	15	16	17	20	25	30	35	4m/s
Baseline (Nm)	117,9	85,7	244,0	131,9	369,0	323,5	309,0	336,3	201,4	178,4	163,3	139,3	
With 20% blf (Nm)	118,9	85,8	279,9	155,6	409,3	411,2	401,3	387,2	210,2	190,0	172,5	148,3	
Increase %	0,9	0,1	12,8	15,2	9,8	21,3	23,0	13,1	4,2	6,1	5,4	6,1	10,65

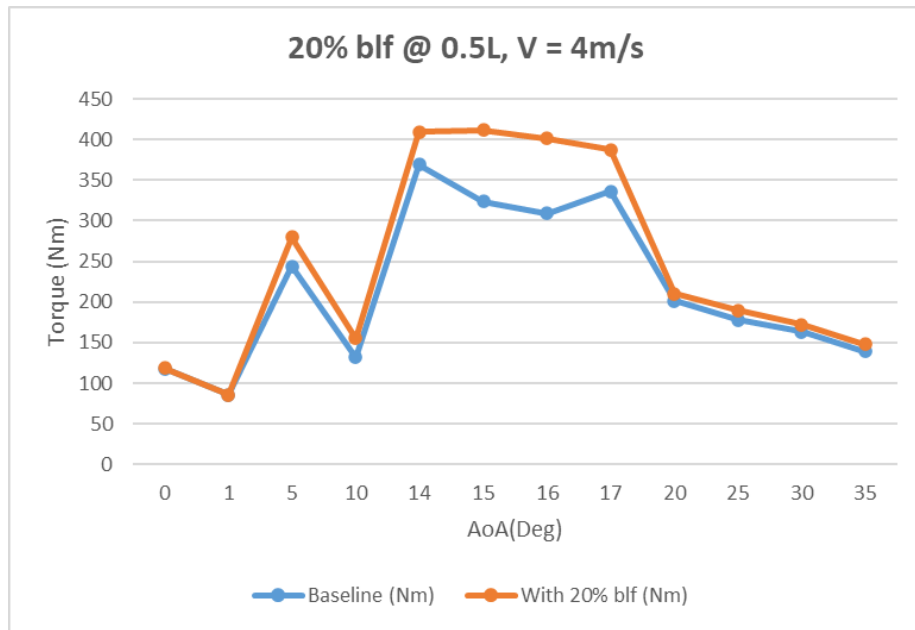


Figure 5-16 : Results of 4m/s performance increase (baseline vs 20%blf @ 0,5L). (Author's work)

Table 5-8 : Results of CFDs without a blf installed and the 20% blf installed at turbine blade length L x 0,5, applied to all AoA at wind speed 7m/s. (Author's work)

	20% blf @0.5L, applied to all AoA @ V = 7m/s												V
AoA (Deg)	0	1	5	10	14	15	16	17	20	25	30	35	
Baseline (Nm)	-86,3	74,4	739,9	403,9	1117,6	1229,4	653,2	1044,3	619,3	550,2	499,9	425,9	7m/s
With 20% blf (Nm)	-76,3	83,1	804,7	492,9	1247,0	1265,3	781,5	1152,5	632,4	559,2	522,1	433,8	
Increase %	-13,1	10,4	8,1	18,1	10,4	2,8	16,4	9,4	2,1	1,6	4,3	1,8	7,75

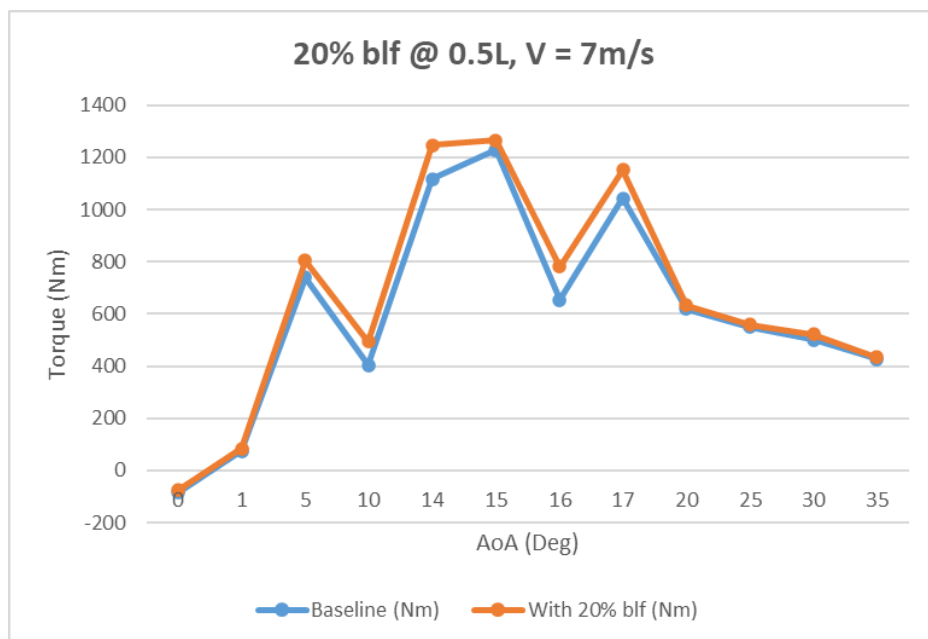


Figure 5-17 : Results of 7m/s performance increase (baseline vs 20%blf @ 0,5L). (Author's work)

Table 5-9 : Results of CFDs without a blf installed and the 20% blf installed at turbine blade length L x 0,5, applied to all AoA at wind speed 10m/s. (Author's work)

	20% blf @0.5L, applied to all AoA @ V = 10m/s												V
AoA (Deg)	0	1	5	10	14	15	16	17	20	25	30	35	10m/s
Baseline (Nm)	734,2	446,2	1515,2	828,7	2261,9	2031,9	1944,3	2099,9	1261,5	1113,2	1020,5	870,5	
With 20% blf (Nm)	733,0	457,2	1672,3	1022,1	2701,0	2556,7	2034,3	2111,6	1301,1	1184,1	1100,0	879,3	
Increase %	-0,2	2,4	9,4	18,9	16,3	20,5	4,4	0,6	3,0	6,0	7,2	1,0	8,16

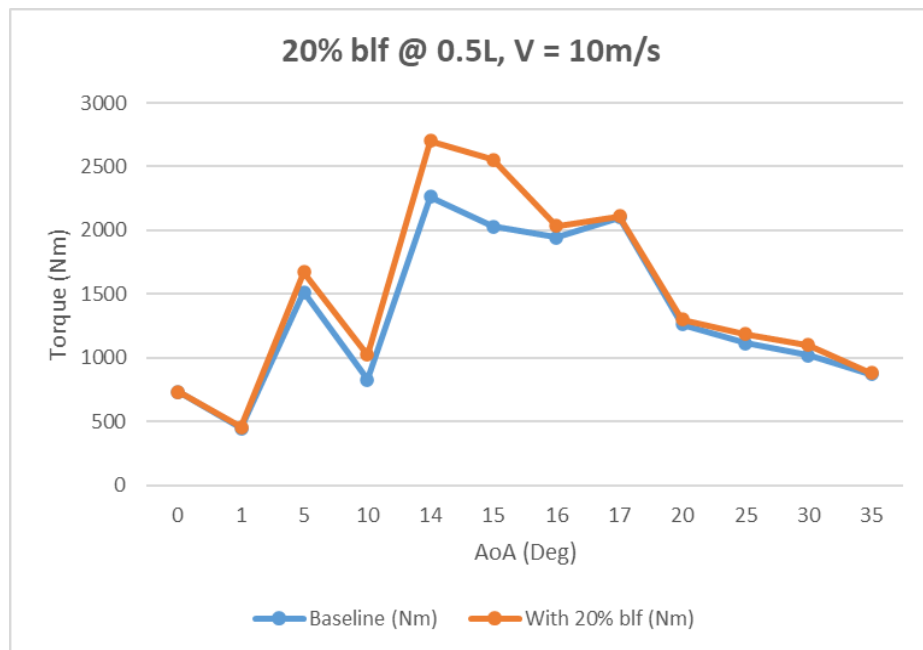


Figure 5-18 : Results of 10m/s performance increase (baseline vs 20%blf @ 0,5L) (Author's work)

Table 5-10 : Results of CFDs without a blf installed and the 20% blf installed at turbine blade length L x 0,5, applied to all AoA at wind speed 13m/s. (Author's work)

	20% blf @0.5L, applied to all AoA @ V = 13m/s												V
AoA (Deg)	0	1	5	10	14	15	16	17	20	25	30	35	13m/s
Baseline (Nm)	-317,8	620,5	2950,1	1401,0	3824,6	4214,0	2954,8	2899,7	2121,9	1889,1	1725,0	1467,3	
With 20% blf (Nm)	-319,7	657,3	3155,9	1655,1	4372,0	4333,1	3777,0	3001,0	2298,0	1977,5	1805,0	1508,1	
Increase %	0,59	5,59	6,52	15,35	12,52	2,75	21,77	3,38	7,66	4,47	4,43	2,70	7,92

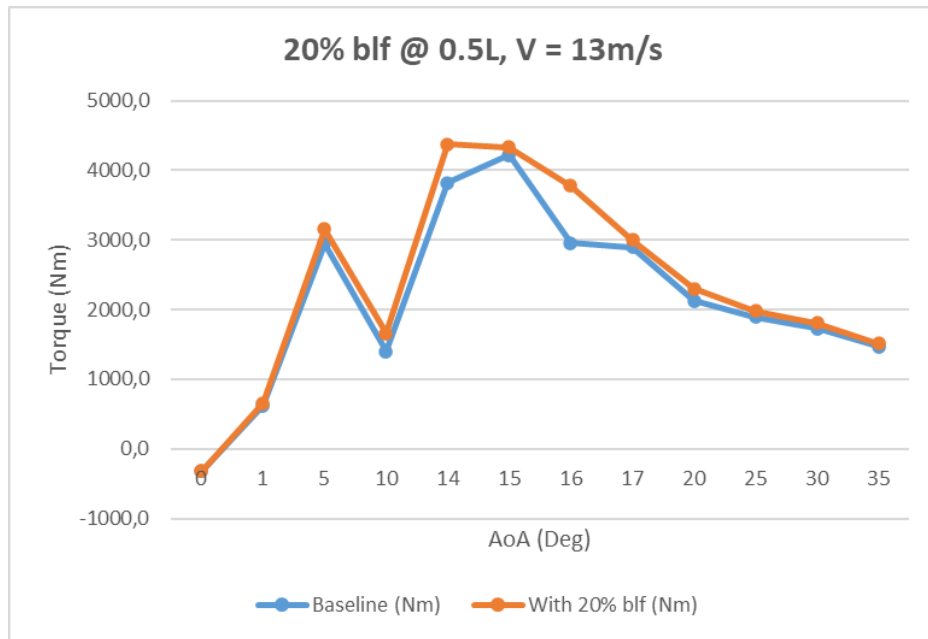


Figure 5-19 : Results of 13m/s performance increase (baseline vs 20%blf @ 0,5L). (Author's work)

Table 5-11 : Single Fence Comparison - Results of the CFDs with the installation parameters No blf and Single blf). (Author's work)

Single Fence comparison			Improvement (%)
V (m/s)	No blf (Nm)	20% blf @ 0.5L (Nm)	
4	323,51	411,2	21,33
7	1229,42	1265,31	2,84
10	2031,9	2556,73	20,53
13	4214,01	4333,06	2,75
Average Improvement			11,86

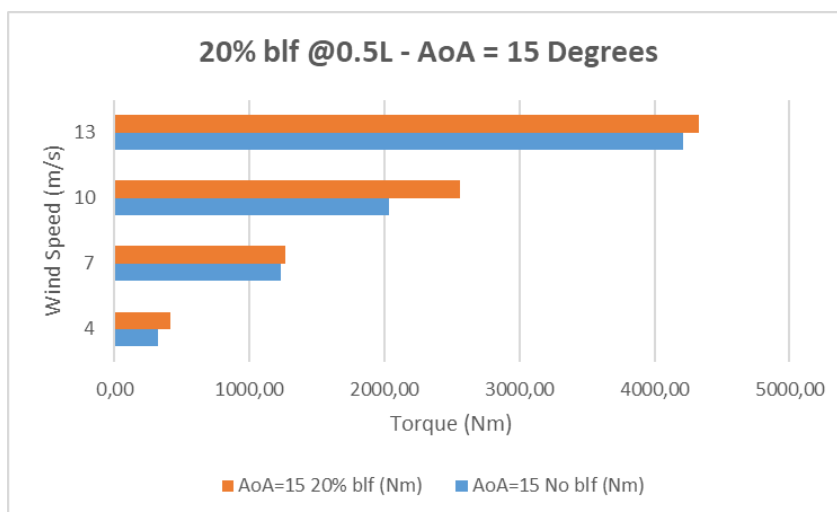


Figure 5-20 : Summary of results (baseline vs 20%blf @ 0,5L). (Author's work)

From the results obtained from the baseline analysis and shown in Figures 5-6 and again in Figures 5-16, 5-17, 5-18, and 5-19, the conclusion can be drawn that the best performance parameters for the rotor in terms of angle (with and without a blf) is at $AoA = 15$ degrees. Hence the best comparative analysis can be done at the critical angle of each rotor. The results tabulated in Table 5-5 can be used as the improvement average for the rotor at the critical angle.

Dual Boundary Layer Fence Application – Rotor 1



Figure 5-21 : NREL 400kW blade – Attached to a generic hub with fences at 50% and 90% of the full length of the blade. (Author’s work)

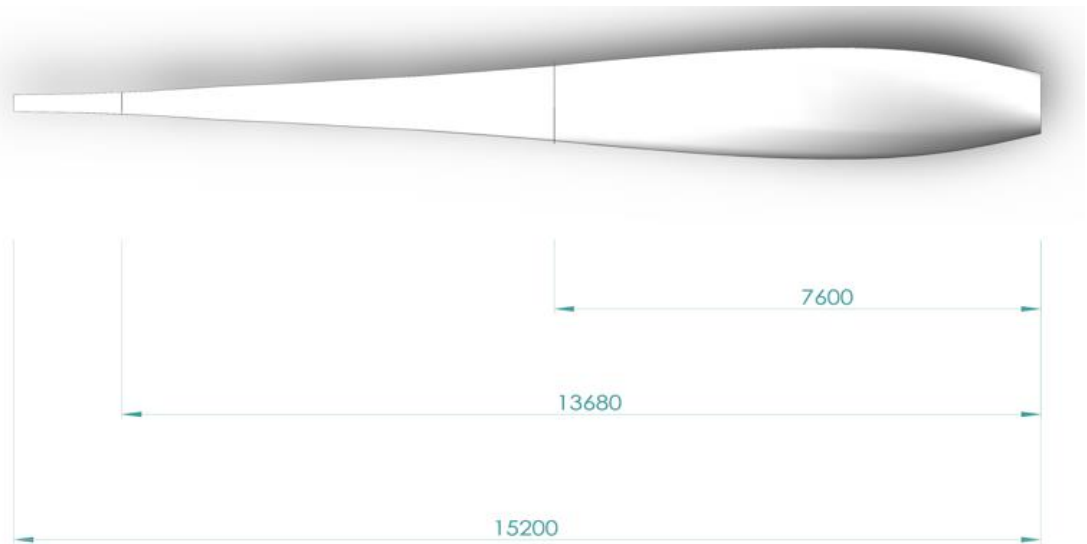


Figure 5-22 : NREL 400kW blade – Showing the location of the fence installations = 50% and 90% of the full length from root to tip. (Author’s work)



Figure 5-23 : NREL 400kW blade – Showing the full blade with 20% augmented fences installed as per the results of the fence height analysis. (Author’s work)

For the blf installed at 90%, the same design principle was applied. The thickness of the aerofoil at the 90% section is 53mm, hence $(53\text{mm} \times 20\%)$ the blf height is 10,6mm or 11mm rounded up.

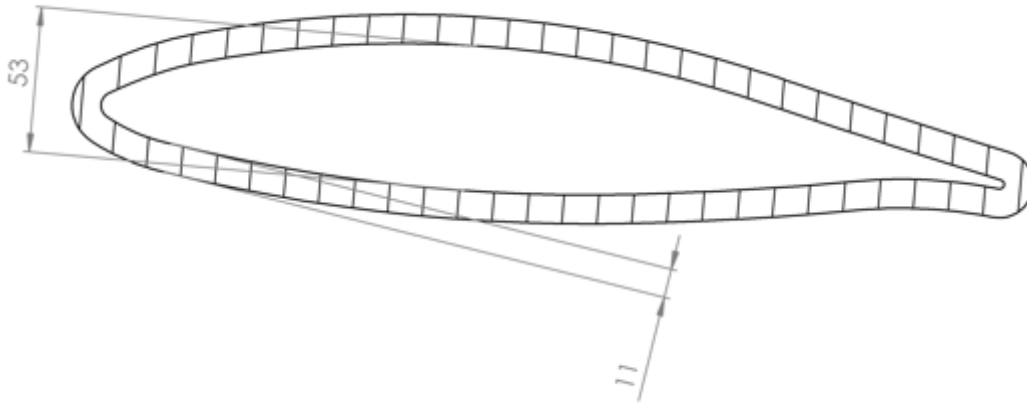


Figure 5-24 : NREL 400kW blade – Showing aerofoil section at 90% of blade length with 20% augmented fence. (Author’s work)

After the CFD study has been completed on the dual blf installation, we can now confirm that the second blf did not increase the torque output significantly as per Durga & Balaji (2016).

As shown in the table below, the improvements only amounted to 1% on average, which can still be worth the investment in conjunction with a blf at 50% of the length of the blade.

Table 5-12 : Fence Comparison - Results of the CFDs with all the installation parameters in this study (No blf, Single blf and Dual blf). (Author’s work)

Fence comparison				Improvement (%)
V (m/s)	No blf (Nm)	20% blf @ 0.5L (Nm)	20% blf @ 0.5L and 0.90L (Nm)	
4	323,51	411,20	412,89	1,00
7	1229,42	1265,31	1264,41	1,00
10	2031,90	2556,73	2560,97	1,00
13	4214,01	4333,06	4338,90	1,00

5.3 Blade selected for the verification/follow-up CFD study.

Rotor -2 Data

For the research study, the 1000kW, National Research Energy Laboratory (NREL) blade with the below detail was selected. The second blade is less complex than the first. It has only 1 x type of aerofoil and has a 0° twist between the root and tip.

Blade Length	= 26.5m
Aerofoils Profile	= NREL S830
Blade Twist	= 0 Degrees between root and tip
Maximum Chord Length	= 3m
Critical Angle	= 16 Degrees
Cut-in speed	= 3m/s
Rated speed	= 14m/s
Cut-out speed	= 25m/s
Power Curve	= Not available for the specific unit.
Position of each Blade Element	= Please see "Appendix C"

Information obtained from Velazquez et al., (2014)



Figure 5-25 : NREL 1000kW blade – Attached to a generic hub (Velazquez et al., 2014)

Baseline Torque Analysis – Rotor 2

The baseline analysis was conducted to assess the initial output values and characteristics of the turbine blade in its original, unmodified state. According to the datasheet provided, the cut-in wind speed, which is the minimum wind speed required for the turbine to start generating power, is 3 m/s. This wind speed was selected as the first input condition for the baseline performance analysis of the turbine blade. For the analysis of the second rotor, AoA = 0° , 5° , 7° , 10° , 13° , 16° , 18° and 20° , was used to get the baseline performance parameters at each selected wind speed.

The baseline analysis was done for each wind speed (3, 7, 10, 14m/s) as indicated in the methodology. Each graph was plotted separately.

The airflow was applied perpendicular to the blade.

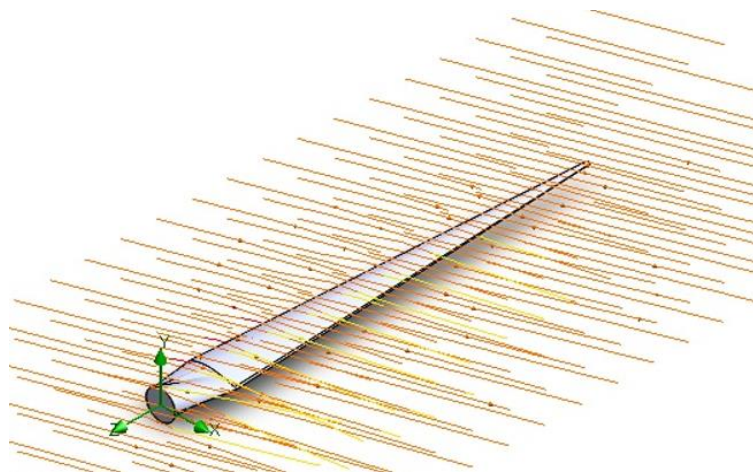


Figure 5-26 : NREL 1000kW blade – Showing CFD airflow applied perpendicular to the blade. (Author's work)

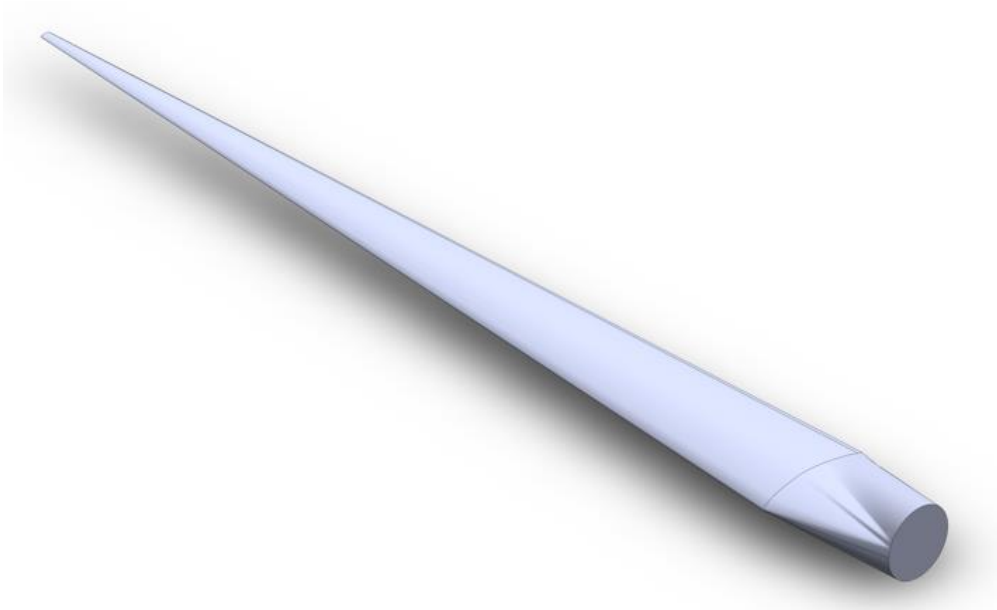


Figure 5-27 : NREL 1000kW blade – Attached to a generic hub. (Author’s work)

The selected NREL 1000kW blade has 0° twist from the root to the tip of the blade. The blade design starts with a cylinder and transitions into a S830 aerofoil. The blade only features an S830 aerofoil from the transition section to the tip.

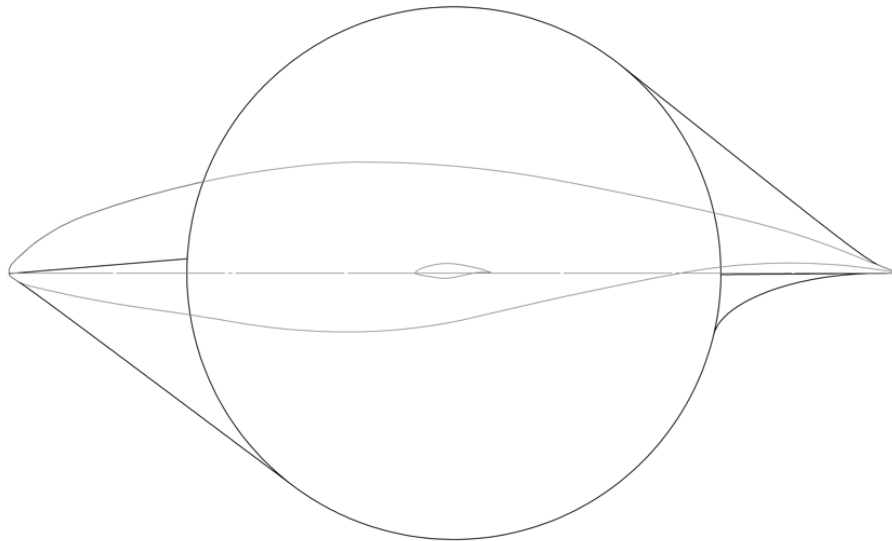


Figure 5-28 : NREL 1000kW blade – Showing aerofoil makeup and a twist of the blade. (Author’s work)

The baseline torque analysis for the 1000kW rotor confirmed the known data of the blade. The cut-in wind speed was confirmed to be around 3m/s and the critical angle of attack to be approximately 16 degrees. The data shows a sharp increase in torque generation around 16 degrees and then a sudden drop.

Table 5-13 : 1000kW NREL - Tabulated baseline performance at all selected wind speeds. (Author's work)

Baseline Torque Analysis									Torque output (Nm)
V (m/s)	Angle of Attack (AoA)								
	3	5	7	10	13	16	18	20	
3	806,25	1347,96	2067,46	1411,45	1099,86	1322,61	1264,54	1352,93	
7	3534,92	4266,45	6368,51	4307,70	3966,33	14951,73	3976,40	17185,24	
10	1831,31	8897,69	13225,87	8889,99	6879,98	30672,69	7796,40	35509,08	
14	15731,03	15422,80	20057,49	14913,38	13556,15	55030,99	14046,54	14913,38	

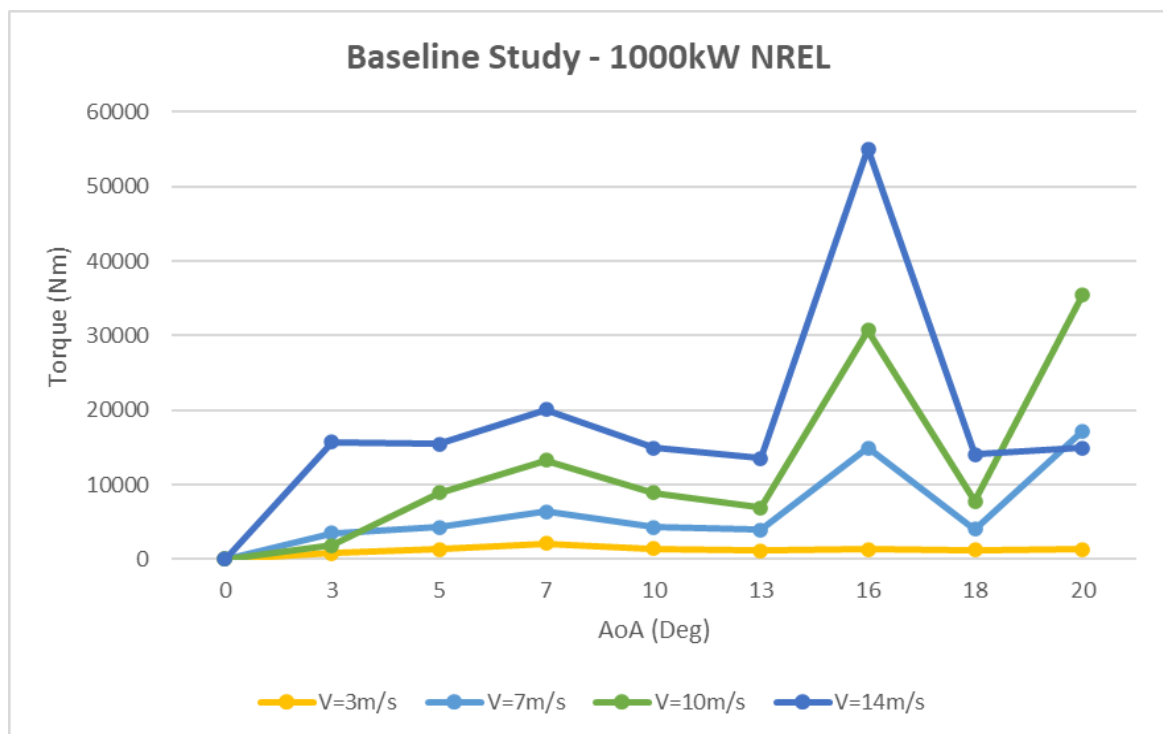


Figure 5-29 : 1000kW NREL - Baseline performance at all selected wind speeds. (Author's work)

Single Boundary Layer Fence Application – Rotor 2

The second rotor's analysis is used for verifying the method of augmentation derived in the first sections of this study. Hence, the SFA or single fence augmentation method was applied. This means that the fence was installed at 50% of the blade length and the fence height is 20% of the maximum thickness of the aerofoil.

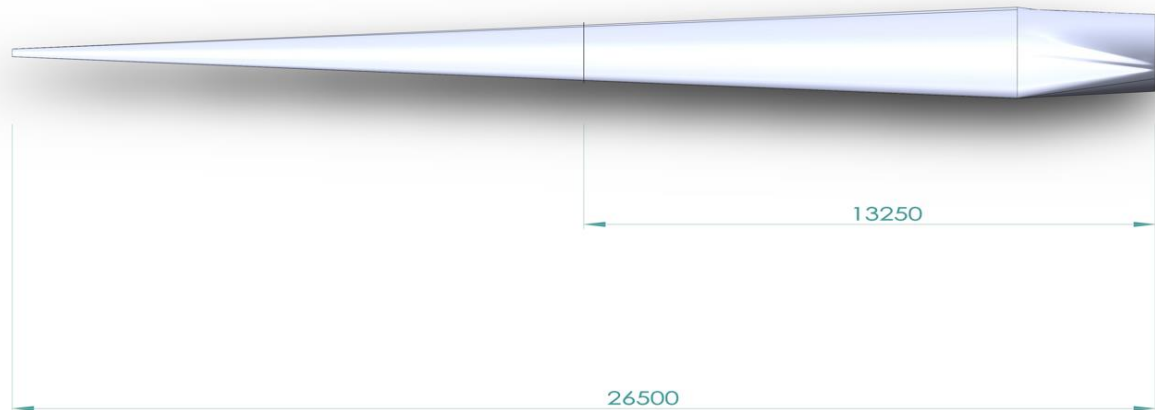


Figure 5-30 : NREL 1000kW blade – Showing the location of the fence installation = 50% of the full length from root to tip. (Author's work)

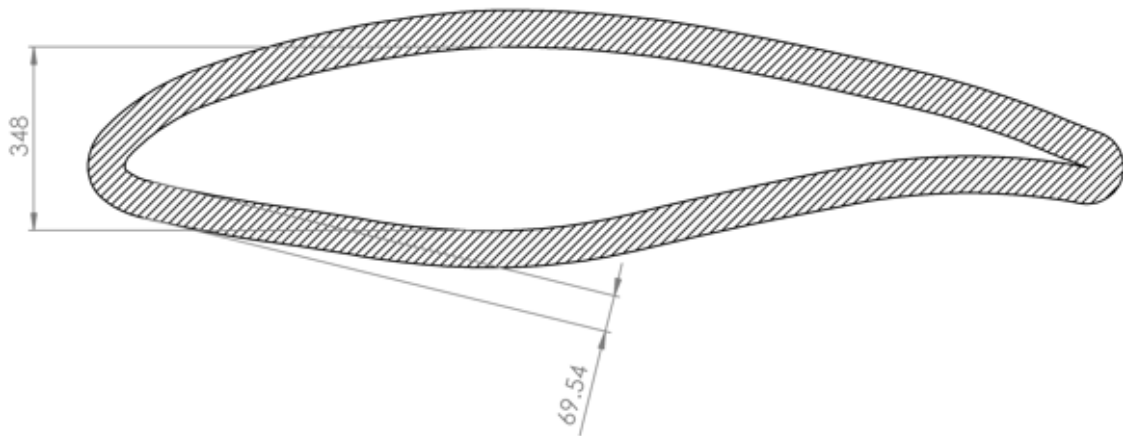


Figure 5-31 : NREL 1000kW blade – Showing aerofoil section at 50% of blade length with 20% augmented blf. (Author's work)

Table 5-14 : NREL 1000kW blade – Result comparison between “No blf” and “20% blf” at AoA = 16 Degrees (Critical angle). (Author’s work)

1000kW NREL blf 20% @ 0.5L			
AoA = 16 Degrees			
V (m/s)	No blf (Nm)	20% blf (Nm)	Increase %
3	1322,61	1409,11	6,54
7	14951,73	16247,30	8,67
10	30672,69	33814,58	10,24
14	55030,99	61558,52	11,86
Ave			9,33

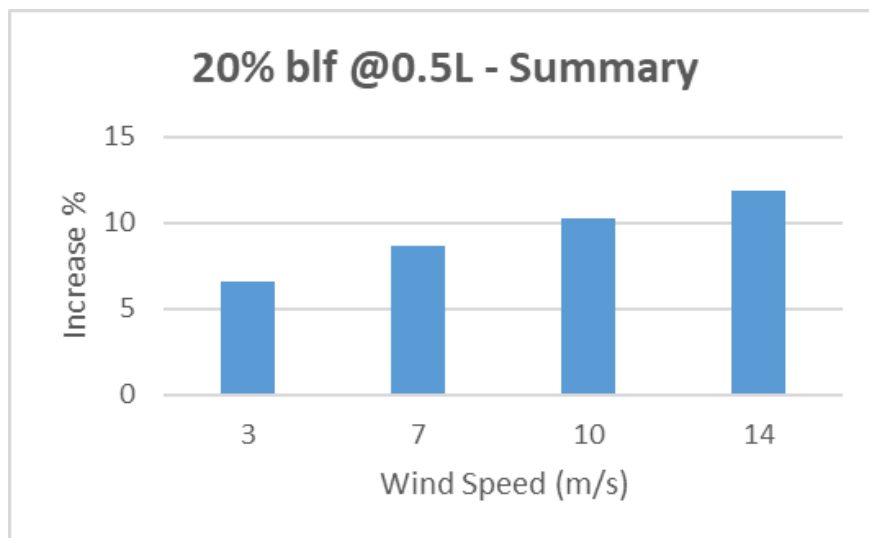


Figure 5-32 : NREL 1000kW blade – Improvement results after installing a 20% blf. (Author’s work)

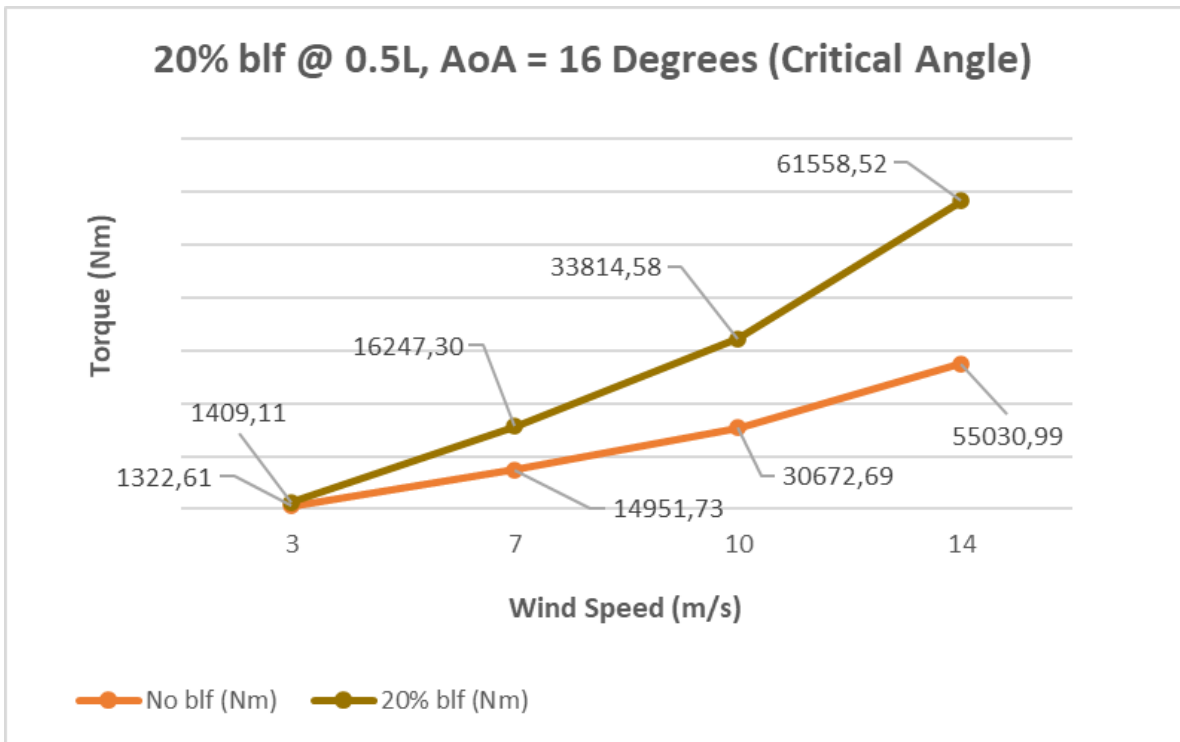


Figure 5-33 : NREL 1000kW blade – Graph showing how the improvement results after installing a 20% blf (Author’s work).

5.4 Results

Single Fence Augmentation Method or SFA

The SFA method applied to 2 x rotors, produced a result of an average increase in torque of 9.33 – 11.86% from the baseline values. This is a significant improvement in the aerodynamics of the blades. However, it was not the only objective achieved, the CFD analysis was also used to investigate the blf height that would produce the maximum torque increase when placed 50% or halfway between the root and tip of the blade. The result was that if you measure the aerofoil thickness at any section of the blade, the most optimized blf at that location would have a height of 20% of the aerofoil thickness. This standard augmentation method allows the spanwise airflow elements created by the centrifugal forces during the rotation of the rotor, to be diverted in the axial direction, over the blade allowing the rotor to generate more torque.

The SFA method is mathematically expressed in the figure below. It can be simply explained as:

“Placing a blf 50% or halfway between the root and the tip of a blade, making the blf height 20% of the specific aerofoil thickness at the halfway location”.

$$SFA = \Delta L(x) + \Delta t(y)$$

Equation 5-1 : Mathematical expression of Single Fence Augmentation method (Author's work).

Where:

- L = Full length of the wind turbine blade (from root to tip)
- t = thickness of the aerofoil at the specific location
- x = 50% or 0.5
- y = 20% or 0.2

(x) and (y) are constants.

The idea of the SFA method is to increase the torque or power output of a rotor by a predictable amount without doing in-depth analysis or calculations. Thus far, the predictable value is between 9.33 and 11.86% of the baseline torque or power. This method captures the spanwise airflow elements in the first half of the blade only.

Dual Fence Augmentation Method or DFA

The DFA method of augmentation is an extension of the SFA method. This method adds a second blf to the blade at 90% of the blade length towards the tip. The blf height is also determined by measuring the aerofoil thickness at 90% and making the height 20% of the thickness. This method captures the spanwise airflow elements between 50 and 90% of the blade. However, the results show that there is not much energy left to extract from this section if the 50% blf captures the bulk of the flow elements. This method of augmentation was only applied to the first rotor in the study and produced an average increase torque of 1%. This 1% does not seem like a significant improvement, but when the value of this implementation is equated with the value of the South African wind energy sector, it can be of significant value.

The DFA method is mathematically expressed below:

$$DFA = [\Delta L(x) + \Delta t_1(y)] + [\Delta L(x') + \Delta t_2(y)]$$

Equation 5-2 : Mathematical expression of Dual Fence Augmentation method. (Author's work)

Where:

L	=	Full length of the wind turbine blade (from root to tip)
t_1	=	thickness of the aerofoil at the 50% position.
t_2	=	thickness of the aerofoil at the 90% position
x	=	50% or 0.5
x^i	=	90% or 0.9
y	=	20% or 0.2

Only (y) is a constant.

With both the SFA and DFA methods, a clear increase in torque generation can be noted. However, one of the objectives of the research was to ascertain if the cut-in speed and the critical angle can be improved.

6. CHAPTER SIX

ECONOMIC IMPROVEMENT IN A SOUTH AFRICAN CONTEXT

6.1 Status Quo in South Africa, September 2023

The South African wind energy industry stands as one of the significant opportunities for the country to grow economically while ensuring its transition to a greener, more sustainable future. The local government has identified the benefits of renewable energy and initiated ambitious plans to increase its share in the national energy mix. The expansion plans for wind energy deployment are expected to attract significant investments, create jobs, and foster local economic growth.

The government has set a target of achieving 18.8 GW of renewable energy by 2030, which includes the installation of 14.4 GW of wind energy capacity. To achieve this target, a large number of wind farms are in various stages of development across the country. If all the proposed wind farms are constructed by 2030, it will create a significant impact on the South African economy.

One of the primary ways in which the South African wind energy industry can contribute to economic growth is by creating employment opportunities. The wind energy projects will require a skilled workforce, from engineers and technicians to project managers and administrative staff. With the establishment of new wind farms, thousands of people will experience employment opportunities, leading to the development of local communities. Additionally, the government's prioritization of inclusive economic growth ensures that local communities where wind farms are established will be involved in the procurement, development, and operation of wind energy facilities.

Another significant contribution of the wind energy industry to the South African economy is the generation of foreign direct investment. The development of wind projects in the country offers an opportunity for foreign investors to put their capital into the market. The investments received will create a multiplier effect, with development banks, financiers, equipment suppliers, and other stakeholders participating in the industry.

Apart from job creation and investments, wind energy projects can also trigger regional economic development. The development of new wind farms requires extensive infrastructure, including transmission lines, access roads, and substations. This leads to investments in local infrastructure and service development, such as hotels and utilities, creating opportunities for small and medium enterprises, which has a positive cascading effect on economic activity, leading to the growth of local economies.

Wind energy's contribution to socioeconomic development is not limited to employment and investment. It has a direct impact on energy costs, particularly in rural areas where grid electricity is scarce. Large-scale wind energy facilities can significantly reduce the cost of

electricity due to their low operating costs, thus providing affordable and reliable power for local communities, thereby increasing the standard of living.

In conclusion, the South African wind energy industry has a significant potential impact on the country's economic growth. If all the planned wind farms are constructed by 2030, it will generate a substantial boost to the economy through employment, foreign direct investment, and regional growth. Therefore, whilst ensuring the transition to a green energy future, it is essential to maximize this opportunity to contribute to the country's socioeconomic development.

The South African Wind Farm Program (SAWEP) originated in June 2000 when the Darling Wind Farm was declared a National Demonstration Project. The farm was built with 4 x German-designed wind turbines, each with a generation capacity of 1.3MW (5.2MW total) with an expected annual output of 13.2GW @ 28% load factor. This was the first grid-connected, independent wind farm developed in South Africa (energy.gov.za)

According to the Department of Energy (DOE), as of 2023, South Africa has 37 operating wind farms with an installed capacity of 3560 MW. The Renewable Energy Independent Power Producer or REIPP is a tender process, implemented by the DOE where the most cost-effective tariff and competitive Economic Development score could result in a 20-year Power Purchase Agreement or PPA. This agreement is signed with Eskom (South African state utility).

The tender was implemented in various rounds, and as of 2023, 6 x rounds of the REIPP tender have been closed.

The wind energy allocated through these tenders is as follows:

Bid Window 1 – 634MW (Minister Remarks IPP Bids Announcement, 2011)

Bid Window 2 - 562.5MW (Preferred Bidders – Window 2, 2013)

Bid Window 3 – 787MW (Bid Window 3 Preferred Bidders' announcement, 2013)

Bid Window 4 – 676MW and an additional 687MW was added. (Minister of Energy - Media Statement, 2015)

Bid Window 5 – 784MW (Ministers REIPP announcement, 2022)

Bid Window 6 – 3200MW (Ministers REIPP announcement, 2022)

This means that the REIPP allocated wind energy total sits at 6643.5MW

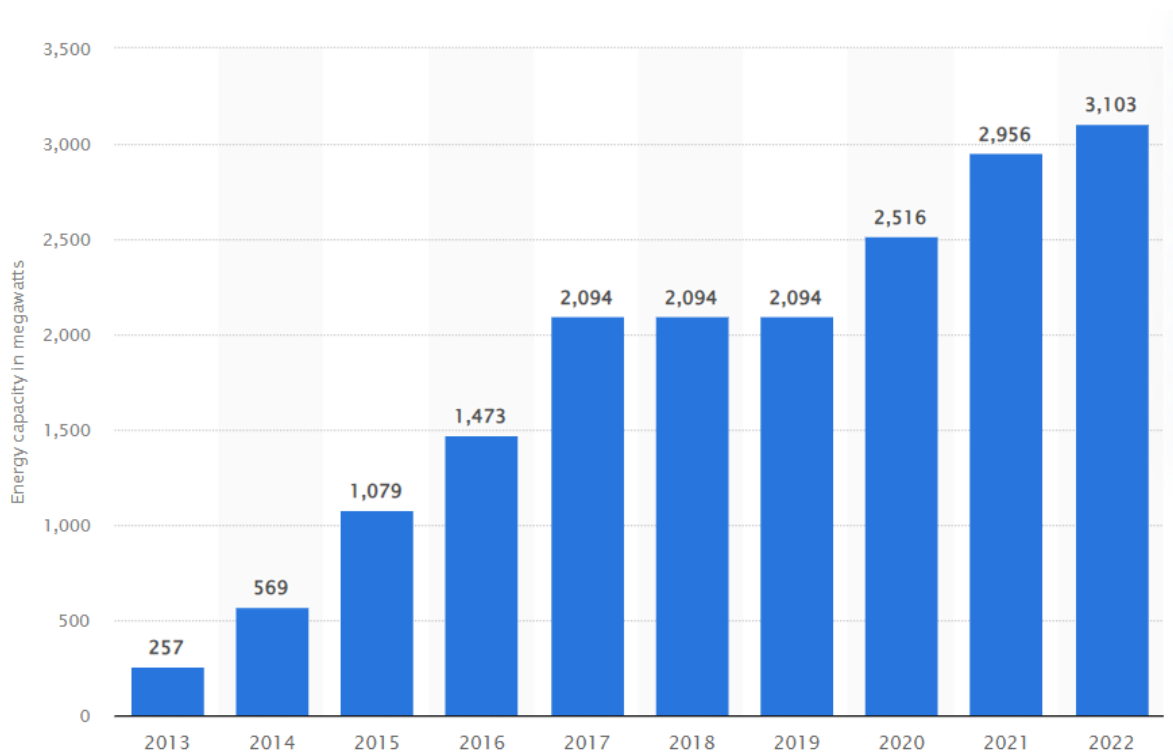


Figure 6-1 : Total wind energy capacity in South Africa from 2013 to 2022, (Statista, 2023)

6.2 The possible application of the improvement method

The Sere Wind Farm, outside Vredenburg in the Western Cape of South Africa, has a nameplate capacity of 100MW. This farm has 46 x 2.3MW wind turbines installed on a 16km² property and was built and commissioned in 2014 at a total cost of ZAR 2,689 billion (African Development Bank Group, 2015).

ZAR = South African Rand.

The cost of estimating a wind farm budget is a very complex task that involves the cost of manufacturing the components, transportation, installation operations, and maintenance for the first 10 years (George Duval, 2023).

According to Duval (2023), the cost of manufacturing the turbine could be as much as 70% of the total cost, and transport could account for 3 to 8%, depending on the location of the site. The installation cost varies the most for specialized equipment and labour.

The simplified estimation method used to make an approximate estimate determination for wind farm projects' "ballpark budgets" is as follows (Duval, 2023):

Cost /MW = Project Value / Nameplate Capacity.

Thus, it can be estimated that at Sere Wind Farm, the cost was = ZAR 26 890 000/MW. Windpower Engineering & Development (2019) estimates that the total cost of wind power projects is reduced by 6.41% per year and has done so over 5 years before 2019. The average cost of installation in South America was USD 0.5 million/MW and USD 1.7 million/MW in Asia. This coincided with the US average of USD 1 million/MW.

1 USD is worth ZAR 18.87 on 21 September 2023.

Seriti Green is currently (Q3, 2023) constructing a 155MW wind farm in Mpumalanga South Africa that will cost ZAR 4 billion (SAWEA, 2023), this budget can be reduced to ZAR 4 000 000 000/155MW = ZAR 25 806 000/MW, which is within a very close margin of what the Global estimation is and what Sere Wind Farm's budget was.

In South Africa, using the above scenarios, it can be conservatively estimated that for project budgeting purposes, the cost will be in the realm of ZAR 26 000 000/MW and for savings calculation purposes we can use USD 1 million/MW which translates to roughly ZAR 19 000 000/MW on 21 September 2023.

Wind Capacity Factor

In South Africa, the wind capacity factor calculator (WCFC) was developed to estimate the annual wind energy production at any location in the country. South Africa has the CSIR PV/wind aggregation and the Wind Atlas for South Africa (WASA) datasets. These two datasets have a degree of error of less than 5%, hence both are suitable for estimating the wind energy output (Kekana & Landwehr, 2019). From research conducted by Kekana & Landwehr (2019), it was found that the location and height of the wind turbine all contribute to the wind capacity factor (CF) results. Kekana & Landwehr (2019) took data from 4 separate locations in South Africa. According to Adefarati & Obikoya (2019), Cape Town was found to be the most suitable for the installation of wind turbines with a CF of 22.1% at 50m hub height. A more recent study by Karamanski & Erfort (2023) on the performance of active wind farms in South Africa, revealed that there are some wind farms with CF's as high as 41.85% (Noupoort) and the lowest having a CF of only 19.19% (Darling). The study also revealed that South Africa has an overall CF of 33.43%, which can be compared to that of the United States of America at 34.6%. This also puts South Africa well above the global average of 25%.

The capacity factor (CF) = actual output/ maximum possible output, where the maximum hours per year is 8760 hours (Kasper, 2023).

Possible improvement of the performance of future installations in South Africa.

Taking the above estimations into account and integrating them with the Single Fence Augmentation (SFA) method, it can be estimated that a wind farm can perform 9.33% better in terms of power output in the same wind application parameters. This translates into the estimations below:

Using Seriti Green's planned project in Mpumalanga mentioned above, the 155MW wind farm could have a 9.33% better output, changing the nameplate rating to 169.5MW for the same ZAR 4 000 000 000 budget.

The cost of modifying the blade design to include a blf on a new turbine blade that has not been installed yet, adds <1% to the material volume (drawn off the 3D model), hence it could be estimated that the manufacturing cost would be <1% more expensive on material alone.

Using Seriti Green's planned project in Mpumalanga again, instead of building a 155MW conventional wind farm, they could use blf modified wind turbines and build a 155MW wind farm at the cost of a 140.5MW wind farm. This would result in a 14.5MW saving at an estimated cost of ZAR 19 000 000/MW as stated above (Total saving = ZAR 275 500 000).

$$(155MW - 9.33\% = 140.5MW)$$

Possible improvements of in-service installations in South Africa.

The estimation of what a 9.33% increase could result in, for an older wind farm is difficult to estimate. However, by applying the SFA method to all the in-service wind farms in South Africa, increasing the national output of all wind farms from 3142.5MW (Nameplate rating, Appendix A) to 3435.7MW could be significant. The installation cost of blfs on all in-service wind turbines (1437, Sept 2023) must be investigated as the environment at every site, and method of installation, make estimating the cost difficult. The result could be a 293.2MW change in nameplate rating (9.33% output increase) added to the national grid at a relatively low cost, as opposed to building a 293.2MW wind farm at an estimated cost of ZAR 19 000 000/MW (293.2 x ZAR 19 000 000/MW = ZAR 5,57 billion). The total cost saving could be significant enough to investigate.

Taking the estimated wind capacity factor into consideration, adding 293.2MW to the national grid could result in adding **858 626.82 MWh/yr** or **858 626 820 kWh/yr** to the national grid.

$$(293.2MW \times 8760hrs \text{ annually} = 2\,568\,432 \text{ MWh/yr} \times CF\,33,43\%).$$

The average electricity tariff for municipalities and non-municipalities in 2023/2024 for Eskom was 173,80 c/kWh or ZAR 1,738/kWh (Eskom Retail Tariff Plan, 2023). Hence the total extra income could be **ZAR 1 492 293 409 annually**.

(858 626 820 kWh/yr x ZAR 1,738/kWh = ZAR 1 492 293 409 (ZAR 1,49 billion).

7. CHAPTER SEVEN CONCLUSION AND RECOMMENDATIONS

Conclusion

This research aimed to develop a standardized method for improving the aerodynamic efficiency of wind turbine rotor blades.

The objectives were to find the most efficient height of the boundary layer fence (blf) and to place the blf in the most invasive position along the length of the blade which would result in the best aerodynamic improvement. The final objective was to be able to express a standardized aerodynamic efficiency improvement method for wind turbine rotors, mathematically.

By modeling known rotor blades (NREL 400kW and NREL 1000kW) on SolidWorks and applying real-world applications to the rotors in the CFD program, a baseline was created for each wind speed at a specific angle of attack. Then a fence was introduced @ 50% of the length of the blade to divert the airflow over the first 50% of the blade. This was found to be the most effective position for a fence placement by Arumugam et al., (2016). Once the fence was placed, the height of the fence was established by increasing the fence height from 5% of the aerofoil thickness to 25%, in 5% increments. The results were tabulated and found that after 20%, the improvements plateaued hence 20% was selected as the most feasible fence height.

Using the above data, the Single Fence Augmentation (SFA) method was derived to standardize the fence installation method. This method yielded results of an 11.86% improvement in the first rotor and 9.33% in the second.

Taking the improvement 1 step further, a second fence was introduced at 90% along the length of the blade and at the same 20% fence height calculation. This only yielded a 1% improvement. This method was called Dual Fence Augmentation (DFA) and a standardized formula could be derived for it. On the low end, the SFA method delivered a 9.33% torque output increase. Adding the second blf or applying the DFA method added another 1% improvement on average. This brings the average improvement to 10.33% overall.

In conclusion, the fence height analysis produced positive results that coincide with deflecting or diverting the spanwise airflow elements between the root and tip, as well as the vorticity vectors over the blade as discussed by Herraez et al., (2016).

A mathematical expression was derived for both SFA and DFA methods.

By applying only the SFA method to a planned wind farm project (new installation) with a known budget, the 9.33% improvement estimation could have significant savings for the developer. In Chapter 6, section 6.2, using Seriti Green's 155MW wind farm project as an example, the 9.33% improvement could yield a 14.5MW saving for the same 155MW nameplate rating. By installing 14.5MW less, the developer could save ZAR 19 000 000/MW = ZAR 275 500 000 on the project.

On old installations, the in-service application of the SFA or DFA method is not as cost-effective as with a new installation, as the fences will have to be installed while the farm is active. This can be costly due to all the factors that could affect the fence installation cost. However, improvement of the output could offset the application cost quickly at each wind farm. By applying the SFA method to all the active wind farms currently in service nationally, the national nameplate rating could go from 3142.5MW to 3435.7MW. This 293.2MW improvement could result in 858 626.82 MW/yr being added to the national capacity, yielding an income of approximately ZAR 1,49 billion/yr at a tariff rate of ZAR 1,738/kWh.

Recommendations

Chapter 6 of this paper is a broad analysis of what a 9.33% output improvement could mean to the wind energy spectrum of South Africa by, September 2023.

For an in-depth study to be completed, both the SFA and DFA improvement methods must be further interrogated and refined.

From a CFD point of view, more emphasis can be placed on the meshing method used for refining the results closer to the surface of the blade and around the blfs.

The SFA method will have to be applied to more wind turbine blades to determine if the improvement specification range remains constant with more than 2 x blade designs.

The DFA method will have to be applied to the same blade designs as the SFA. The DFA method will also have to be applied in different arrangement patterns for placing the blfs. The recommended placement applications are as follows:

- 0.2L and 0.6L (use blf height calculation, as per this study)
- 0.3L and 0.7L (use blf height calculation, as per this study)
- 0.4L and 0.8L (use blf height calculation, as per this study)

For the cut-in speed, the ideal would be to be able to lower the design cut-in speed, to allow the blade/rotor to generate torque from lower wind speeds.

For the critical angle, the ideal would be if clear evidence could be presented for a delay in the stall, thus changing the critical angle.

None of the above could be presented in this study. It is therefore recommended that further studies be focused on proving that the implementation of the SFA or DFA methods could present a lower cut-in speed and a delay in the stall.

As shown in Chapter 5 of this study, the installed blfs @ 20% of the aerofoil thickness are not large applications or installations to the blades, hence the structural integrity of the blades should not be affected. However, this must be verified should an installation be done.

Summary of the Conclusion

By determining the ideal fence height to be 20% of the aerofoil thickness and installing the fences at 50% and 90% of the blade length, the SFA and DFA methods were developed as a quick improvement method for wind turbine rotors. For rotor 1 the output torque improvement results were 11.86% using the SFA method and an extra 1% using the DFA method. For rotor 2 the SFA method yielded a 9.33% improvement in the output torque.

By using the smallest improvement (9.33%) as case study and applying it to the Sereti Green 155MW project discussed in section 6.2, the project developer can build the same 155MW wind farm with 14.5MW less wind turbines. This could result in an estimated ZAR 19 000 000/MW or ZAR 275 500 000 saving.

If the same 9.33% (SFA) improvement is applied to all the currently installed wind turbines in South Africa, then the nationally installed wind capacity could increase from 3142.5MW to 3435.7MW. The difference of 293.2MW could result in an increase of 858.6GW/yr to the national grid.

BIBLIOGRAPHY

- 1) K. P. (2015) 'Experimental Study of Magnus Effect Over an Aircraft Wing', *International Journal of Research in Engineering and Technology*, 04(10), pp. 406–414. doi: 10.15623/ijret.2015.0410066.
- 2) Alsahlan, A. A. and Rahulan, T. (2017) 'Aerofoil design for unmanned high-altitude Aft-swept flying wings', *Journal of Aerospace Technology and Management*, 9(3), pp. 335–345. doi: 10.5028/jatm.v9i3.838.
- 3) Arumugam, S., Subramania, N. P. and Chidambaram, S. (2016) 'Effect of Boundary Layer Fence Location on HAWT Power Performance', *Circuits and Systems*, 07(08), pp. 1177–1189. doi: 10.4236/cs.2016.78101.
- 4) Bortolotti, P., Bottasso, C. L. and Croce, A. (2016) 'Combined preliminary-detailed design of wind turbines', *Wind Energy Science*, 1(1), pp. 71–88. doi: 10.5194/wes-1-71-2016.
- 5) Calitz, J.R. & Wright, J.G. 2021. Statistics of utility-scale power generation in South Africa in 2020. <http://hdl.handle.net/10204/11865>
- 6) Ceyhan, Ö. and Grasso, F. (2014) 'Investigation of wind turbine rotor concepts for offshore wind farms', *Journal of Physics: Conference Series*, 524(1). doi: 10.1088/1742-6596/524/1/012032.
- 7) Coles, D. S., Blunden, L. S. and Bahaj, A. S. (2016) 'Experimental validation of the distributed drag method for simulating large marine current turbine arrays using porous fences', *International Journal of Marine Energy*, 16, pp. 298–316. doi: 10.1016/j.ijome.2016.10.001.
- 8) Deng, G. B. et al. (1991) 'Three-dimensional full Navier–Stokes solvers for incompressible flows past arbitrary geometries', *International Journal for Numerical Methods in Engineering*, 31(7), pp. 1427–1451. doi: 10.1002/nme.1620310713.
- 9) Ghinea, R. A., Bere, P. and Neamtu, C. (2014) 'Improving the Design of a Wind Turbine Blade', 2014 International Conference on Production Research - Regional Conference Africa, Europe and the Middle East and 3rd International Conference on Quality and Innovation in Engineering and Management (Icpr-Aem 2014), (March 2015), pp. 221–226.
- 10) Herter, E. (1979) 'Wind turbine.'
- 11) Institute for Energy Research (no date) 'Offshore Wind Energy: A Very, Very Expensive Electricity Source More Examples of Potential Offshore Wind Projects in the United States'.
- 12) Journal, I. and Computer, O. F. (2013) '© I a E M E Networks', 4(5), pp. 258–266.
- 13) Krishna, M. et al. (2021) 'Performance Evaluation of an Airfoil Fabricated through Additive Manufacturing, using Simulation', (March).

- 14) Lee, S. L. and Shin, S. J. (2020) 'Wind turbine blade optimal design considering multi-parameters and response surface method', *Energies*, 13(7). doi: 10.3390/en13071639.
- 15) Logdberg, O. (2006) 'Vortex generators and turbulent boundary layer separation control', PhD Thesis, (October).
- 16) Lubitz, W. D. and White, B. R. (2004) 'Atmospheric Boundary Layer Wind Tunnel Applications in Wind Turbine Siting', AIAA/ASME Wind Energy Symposium Reno, USA, (June 2014), pp. 4–9.
- 17) Ma, J. et al. (2019) 'Effect of Airfoil Concavity on Wind Turbine Blade Performances', *Shock and Vibration*, 2019. doi: 10.1155/2019/6405153.
- 18) Management, P. (2019) 'Offshore wind. Presentation for Women in Wind Technology Webinar Why offshore wind?', (July), pp. 1–9.
- 19) Mathew, S. (2017) 'Wind Energy Wind Energy', 13th German Wind Energy Conference, 10(October), pp. 1–158. Available at: <http://dx.doi.org/10.1016/B978-0-12-804448-3/00004-9>.
- 20) Menter, F. R. (2009) 'Review of the shear-stress transport turbulence model experience from an industrial perspective', *International Journal of Computational Fluid Dynamics*, 23(4), pp. 305–316. doi: 10.1080/10618560902773387.
- 21) Mig-, T. et al. (1938) 'Wing Fences'.
- 22) Mueller-vahl, H. et al. (2016) 'GT2012-6 9197'.
- 23) Muheisen, A. H., Yass, M. A. R. and Irthiea, I. K. (2021) 'Enhancement of horizontal wind turbine blade performance using multiple airfoils sections and fences', *Journal of King Saud University - Engineering Sciences*, (xxxx). doi: 10.1016/j.jksues.2021.02.014.
- 24) Natili, F. et al. (2020) 'Video-tachometer methodology for wind turbine rotor speed measurement', *Sensors (Switzerland)*, 20(24), pp. 1–15. doi: 10.3390/s20247314.
- 25) NERSA (2020a) 'Concurrence with the ministerial determination on the procurement of new generation capacity from Renewables (Wind and PV), Storage, Gas and Coal technologies', 27(0), p. 59.
- 26) NERSA (2020b) 'Reasons for Decision Concurrence with the Ministerial Determination on the procurement of 2 000MW generation capacity from a range of energy technologies', 27(0), pp. 1–39.
- 27) Nishino, T. and Hunter, W. (2018) 'Tuning turbine rotor design for very large wind farms', *Proceedings of the Royal Society A: Mathematical, Physical and Engineering Sciences*, 474(2220), pp. 1–20. doi: 10.1098/rspa.2018.0237.

- 28) Ochieng, R. (2013) 'The Petroleum Institute', 666, p. 2013.
- 29) Okda, Y. M. El (2015) 'Design methods of horizontal axis wind turbine rotor blades', *International Journal of Industrial Electronics and Drives*, 2(3), p. 135. doi: 10.1504/ijied.2015.072789.
- 30) Patkunam, K. and Yu, W. (no date) 'Pitching wing', pp. 1–16.
- 31) RATHORE, A. S. (2012) 'Aerodynamic Analyses of Horizontal Axis Wind Turbine By Different Blade Airfoil Using Computer Program', *IOSR Journal of Engineering*, 2(1), pp. 118–123. doi: 10.9790/3021-021118123.
- 32) Sarathi, Y. et al. (2015) 'Study on Wind Turbine and Its', 4(1), pp. 249–256.
- 33) SAWEA (2019) 'Sawea Position Paper on Rsa Manufacturing and Local Content Requirements in the Reipppp', (March).
- 34) Schubel, P. J. and Crossley, R. J. (2012) 'Wind turbine blade design', *Energies*, 5(9), pp. 3425–3449. doi: 10.3390/en5093425.
- 35) Sector, V. P. (2012) 'Wind Power', *Green Energy and Technology*, 20(5), pp. 231–256. doi: 10.1007/978-3-642-20951-2_8.
- 36) Sreejith, B. K. and Sathyabhama, A. (2018) 'Numerical study on effect of boundary layer trips on aerodynamic performance of E216 airfoil', *Engineering Science and Technology, an International Journal*, 21(1), pp. 77–88. doi: 10.1016/j.jestch.2018.02.005.
- 37) Sun, Z. et al. (2017) 'Design of the Off Wind China 5 MW wind turbine rotor', *Energies*, 10(6). doi: 10.3390/en10060777.
- 38) De Tavernier, D. et al. (2021) 'Controlling dynamic stall using vortex generators on a wind turbine airfoil', *Renewable Energy*, 172, pp. 1194–1211. doi: 10.1016/j.renene.2021.03.019.
- 39) The World Bank (2020) 'Offshore Wind Technical Potential in South Africa', p. 76.
- 40) Variable, I., Tal, S. and Garcia, T. (2011) '(12) United States Patent (10) Patent No .:', 2(12).
- 41) Yang, Y., Zeng, P. and Lei, L. (2019) 'Aero-structural Investigation of Sesquiplane Wind Turbine Blades', *Energy Procedia*, 158, pp. 779–784. doi: 10.1016/j.egypro.2019.01.206.
- 42) Zhang, Y. (2018) 'Effects of distributed leading-edge roughness on aerodynamic performance of a low-Reynolds-number airfoil: an experimental study', *Theoretical and Applied Mechanics Letters*, 8(3), pp. 201–207. doi: 10.1016/j.taml.2018.03.010.

- 43) Chen TY, Liao YT, Cheng CC. Development of small wind turbines for moving vehicles: effects of flanged diffusers on rotor performance. *Exp Thermal Fluid Sci* 2012;42:136–42.
- 44) Hansen T, Mühle F. Winglet optimization for a model-scale wind turbine. *Wind Energy* 2018;21:634e49.
- 45) Dias do Rio Vaz DAT. et al. (2014) 'An extension of the Blade Element Momentum method applied to Diffuser Augmented Wind Turbines' *Energy Conversion and Management* 87(2014) 1116-1123.
- 46) Khamlaj TA, Rumpfkeil MP. (2018) 'Analysis and Optimization of ducted wind turbines' *Energy* 162 (2018) 1234-1252.
- 47) Vaz JRP, Wood DH. (2018) 'Effects of the diffucser efficiency on wind turbine performance' *Renewable Energy* 126 (2018) 969-977
- 48) Barnard D, Ismail F. (2022) 'CFD Simulation of Horizontal Axiz Wind Turbine Rotor with fitted Guide Ring' *Research Gate*. Doi:105281/zenodo.7366044
- 49) Kale SA, Sapali SN. (2012) 'Comprehensive Evaluation of Innovative Multi rotor Wind Turbines Designs' *IJMET*,pp.730-739.
- 50) Govardhan M. (2012) 'Improvement of Trubine Performamce by Streamwise Boundary Layer Fences' *JAFM*. pp 113-118.
- 51) Sessarego M, Ramos-Garcia N, Shen WZ. (2018) 'Analysis of winglets and sweep on wind turbine blades using a lifting line vortex particle method in complex inflow conditions' *Journal of Physics*. doi:101088/1742-6596/1037/2/022021.
- 52) Fathi B. (2020) 'Applying Spiroid Winglet on The Tip of NREL 5MW Offshore Wind Turbine's Blade to Investigate Vortex Effects' 75^o National ATI Congress. doi: 10.1051/e3sconf/202019708004.
- 53) Khaled M et al. (2019) 'Investigation of small Horizontal-Axis wind turbine performance with and without winglet' *Energy* 187(2019) 115921.
- 54) Sugathapala TM, Withanage SBPB, Wijewardane S. (2020) 'Aerodynamic modelling of simplified wind turbine rotors targeting small-scale applications in Sri Lanka' *Energy for Sustainable Development* 59 (202) 71-82
- 55) Balasubramaniam S. (2013) 'Design of NACA 63215 Airfoil for a Wind Turbine' *IOSR-JMCE*, Volume 10, Issue 2. pp 18-26.
- 56) Islam et al. (2019) 'Comparison and Selection of Airfoils for Small Wind Turbine between NACA and NREL's S series Airfoil Families' *International Journal of Research in Electrical, Electronics and Communication Engineering*, Volume 4, Issue 2. doi:10.5281/zenodo.3520469.

- 57) Herraез I. (2016) 'Detailed Analysis of the Blade Root Flow of a Horizontal Axis Wind Turbine' EAWЕ. doi :10.5194/wes-2015-1.
- 58) Zongheng H et al. (2019) 'Simulation Analysis on the Blade Airfoil of Small Wind Turbine' ICEMEE 295(2019) 012079. doi: 10.1088/1755-1315/295/2/012079.
- 59) S. S. Rodrigues and A. C. Marta, 'On addressing wind turbine noise with after-market shape blade add-ons', Renewable Energy, vol. 140, pp. 602–614, 2019.
- 60) Kekana H. and Landwehr G. (2019) 'Wind capacity factor calculator' Journal of Energy in Southern Africa, Volume 30.
- 61) Kasper D. (2023) 'Wind Energy and Power Calculations' Penn State EM SC 470.
- 62) Adefarati T. and Obikoya G. (2019) 'Evaluation of wind resources potential and economic analysis of wind power generation in South Africa',
- 63) Karamanski S. and Erfort G. (2023) 'Wind Energy Supply Profiling and Offshore Potential in South Africa' Energies, doi:10.3390/en16093368

APPENDICES

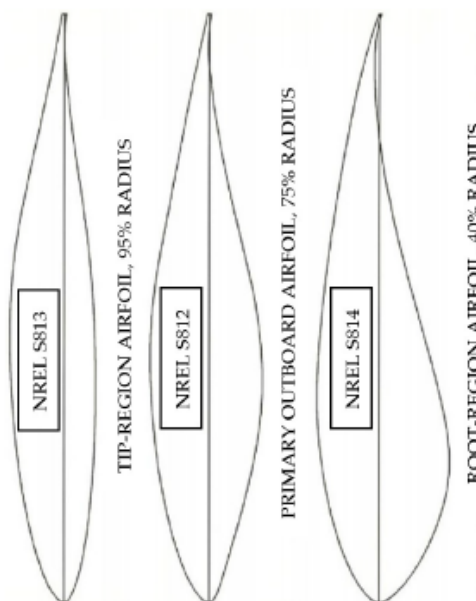
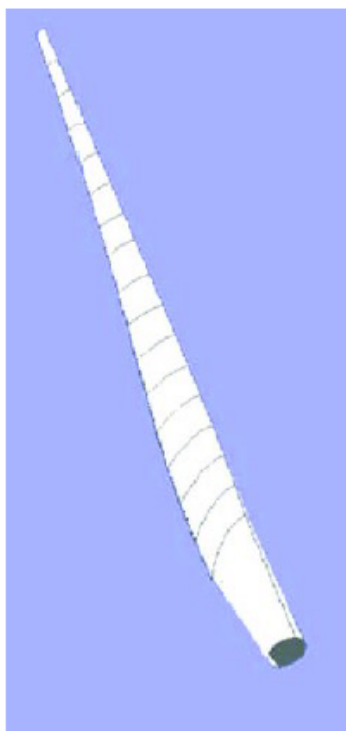
Page left blank on purpose.

APPENDIX A: ACTIVE WIND FARMS IN SOUTH AFRICA, 2023

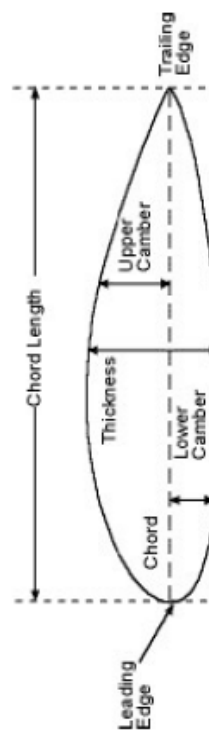
Wind Farm	Province	Turbine Model	Power Capacity (MW)	No. of Turbines	Nameplate Capacity	Commision Year
Amakhala Emoyeni	Eastern Cape	Nordex N117	2.4	56	134,4	2016
Chaba	Eastern Cape	Vestas V112	3	7	21,5	2015
Coega	Eastern Cape	Vestas V90	1.8	1	1,8	2010
Cookhouse	Eastern Cape	Suzlon S88	2.1	66	138,6	2014
Copperton	Northern Cape	Acciona	3.15	34	107,1	2021
Darling	Western Cape	Fuhrländer FL62	1.25	11	13,25	2008
		Fuhrländer FL30	0.25			
Dassieskip	Western Cape	Sinovel SL90	3	9	27	2014
Dorper	Eastern Cape	Nordex N100	2.5	40	100	2014
Excelsior	Western Cape	Goldwind GW121	2.5	13	32,5	2020
Garob	Northern Cape	Acciona	3.15	46	144,9	2021
Gibson Bay	Eastern Cape	Nordex N90	3	37	111	2017
Golden Valley	Eastern Cape	Goldwind	2.5	48	120	2021
Gouda	Western Cape	Acciona	3	46	138	2015
Grassridge	Eastern Cape	Vestas V112	3	20	60	2015
Hopefield	Western Cape	Vestas V100	1.8	37	66,6	2014
Jeffreys Bay	Eastern Cape	Siemens 2.3 MW 101	2.3	60	138	2014
Kangnas	Northern Cape	Siemens 2.3 MW 108	2.3	61	140,3	2020
Karusa	Northern Cape	Vestas V136	4.2	35	147	2022
Khobab	Northern Cape	Siemens	2.3	61	140,3	2018
Loeriesfontein 2	Northern Cape	Siemens	2.3	61	140,3	2017
Longyuan Mulilo De Aar 1	Northern Cape	UPC 86	1.5	63	94,5	2013
Longyuan Mulilo De Aar 2	Northern Cape	UPC 86	1.5	96	144	2013
MetroWind Van Stadens	Eastern Cape	Sinovel	3	9	27	2014
Noblesfontein	Northern Cape	Vestas V100	1.8	41	73,8	2014
Nojoli	Eastern Cape	Vestas V100	2	44	88	2016
Noupoort	Northern Cape	Siemens 2.3 MW 108	2.3	35	80,5	2016
Nxuba	Eastern Cape	Acciona	3.15	47	148	2020
Oyster Bay	Eastern Cape	Vestas V117	3.45	41	147,6	2021
Perdekraal	Western Cape	Siemens SWT-108	2.3	48	110,4	2020
Red Cap Kouga	Eastern Cape	Nordex N90	2.5	32	80	2015
Roggeveld	Western Cape	Acciona AW-125	3	47	147	2022
Sere	Western Cape	Siemens SWT-108	2.3	46	105,8	2014
Soetwater	Northern Cape	Vestas V117	3.3	43	141,9	2022
Tsitsikamma Community	Eastern Cape	Vestas V112	3	31	95	2016
Waainek	Eastern Cape	Vestas V112	3	8	24,6	2015
Wesley-Ciskei	Eastern Cape	Vestas V126	3.45	10	34,5	2021
West Coast One	Western Cape	Vestas V90	2	47	94	2015
Total Nameplate Installed Capacity (MW)					3142,5	2023

The above information was obtained from SAWEA (2023).

APPENDIX B: NREL 400kW BLADE DESIGN

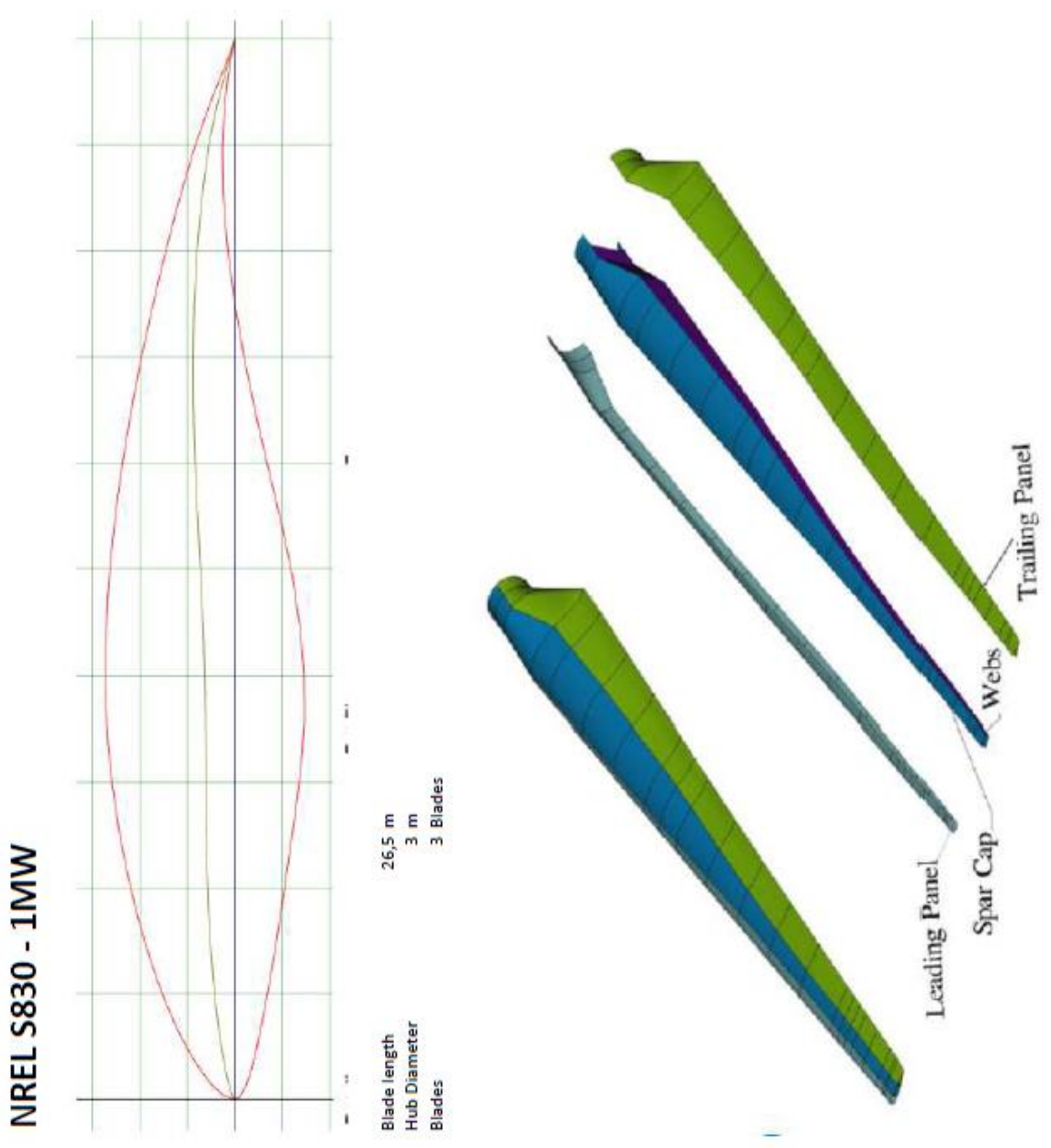


NREL 400kW - 3 Blade					
POS(m)	Chord(m)	Offset(m)	Twist(deg)	Foil	
0	0,9	0	0	Circle	
3,2	1,9	0	0	S814	
4	1,73	0	8,23	S814	
4,8	1,57	0	16,47	S814	
5,6	1,41	0	24,2	S814	
6,4	1,27	0	30,69	S814	
7,2	1,12	0	36,67	S812	
8	1	0	40,91	S812	
8,8	0,88	0	43,89	S812	
9,6	0,78	0	44,87	S812	
10,5	0,69	0	45,11	S812	
11,2	0,6	0	45,09	S812	
12	0,53	0	45,08	S812	
12,8	0,42	0	45,06	S813	
13,6	0,33	0	45,04	S813	
14,4	0,28	0	45,02	S813	
15,2	0,26	0	45	S813	



Information obtained from Cheney & Migliore (1999)

APPENDIX C: NREL 1000kW BLADE DESIGN.



Information obtained from Velazquez et al., (2014)